M 2020

U.PORTO
FEUP FACULDADE DE ENGENHARIA
UNIVERSIDADE DO PORTO

# THE SELECTIVE SEPARATION OF NITROGEN FROM LANDFILL BIOGAS

## DEVELOPMENT OF A TECHNOLOGICAL CONCEPT

**SOFIA RIBEIRO DE SOUSA**

DISSERTAÇÃO DE MESTRADO APRESENTADA
À FACULDADE DE ENGENHARIA DA UNIVERSIDADE DO PORTO EM
ENGENHARIA QUÍMICA

Master in Chemical Engineering

# *Development of a technological concept for the removal of nitrogen from landfill biogas*

## Master dissertation

of

**Sofia Ribeiro de Sousa**

**Developed within the course of dissertation**

held in

**DMT-Environmental Technology/R&D unit**


Supervisor at FEUP: **Dr. Ana Mafalda Ribeiro**

Co-Supervisor at FEUP: **Dr. Alexandre Ferreira**

Coordinator at DMT: **Msc. Benny Bakker**



**April 2021**

# Acknowledgment

The development of a Master thesis within this pandemic context was not ideal. Nonetheless, I can say that I am thankful for these harsher times, since they have shown me how to overcome new challenges and woke me up to all the unconditional support that surrounds me.

To my supervisor at FEUP, Ana Mafalda Ribeiro, I want to express the most sincere and heart-felt “Thank you” for providing me with precious support, guidance and for always pushing me to do better, even when the distance was not in our favor. I would also like to thank Dr. Alexandre Ferreira, for helping me even when he was not obliged to.

To Benny Bakker, my supervisor at DMT, for all the prompt assistance and critical spirit during my internship at DMT. To Gerrit Wigger for his always critical and constructive approach for my problems. I thank you both for always giving me a reason to laugh throughout my days spent in the Netherlands.

To my parents and my brother, I want to express my honest gratitude for all the encouragement and backing not only during this project but during my entire life. Without you, I would not definitely be where I am at today.

To Pedro, my first reader, for supporting me and my dreams, for always loving me through these dark days of Microsoft Word malfunctions and for being patient with me through “thick and thin”.

To Ana Cancela, Maria Vendas and Débora Luíz for acting as a life machine support for me during our 6 months spent together in the Netherlands.

Finally, to all my friends who made this academic journey more meaningful, for all the great moments we lived together, thank you. A special thanks to my best friend, Emanuel, for bringing me breakfast when I needed the most and for all the kindness.

# Abstract

This dissertation is focused on the development of a technological concept for the removal of nitrogen from landfill biogas streams, with an average composition of 80% $CH_4$ and 20% $N_2$, capable of producing bio-methane with high purity (>97%) and recovery (>96%). The adsorption technology conducted in a PSA unit was chosen to perform this separation since it stands out as a mature, economical and efficient process with a large margin for improvement. Moreover, the adsorbent used for this process was the CMS-3K 172, a carbon molecular sieve kinetically selective for $N_2$, although some preliminary studies were also conducted for the Norit RB-3, an activated carbon adsorbent selective at equilibrium for $CH_4$. The highlights of these adsorbents are their commercial availability and reasonable cost, however, CMS usage is desirable due to unnecessary product recompression. Equilibrium and kinetic data were studied for both adsorbents and fitted with Langmuir model.

The software Aspen Adsorption was used to simulate the dynamic behavior of the multicomponent adsorption in a PSA for which a mathematical model capable to accurately predict it was developed. This model was applied in the study of pure-component and binary breakthrough curves of a single column PSA and also in the development and optimization of the behavior of two column PSA processes with 4 steps, 6 steps, 8 steps and vacuum PSA (VPSA) processes with 6 steps and 8 steps.

The breakthrough curves offered an accurate prediction of both adsorbents' performance for which a first estimation of the bed dimensions was made based on the relation between the minimum fluidization velocity, calculated with Ergun equation, and the interstitial velocity. A parametric study was conducted to understand the influence of several operating parameters in the 4-step PSA for which it was revealed that within the ranges of parameters values studied, the enhanced overall performance is delivered when changing the coefficient CV of the product valve and the ratio of the interstitial velocity to the minimum fluidization velocity. Based on this, a 6-step cycle with pressure equalization step as well as an 8-step with pressure equalization and co-current blowdown steps cycle for a PSA and a VPSA were optimized with the criterium of fixing the $CH_4$ purity at 97% to enhance the recovery of $CH_4$ to the maximum possible. The attained results were 97, 97.15, 96.97, 96.92 and 97% $CH_4$ purity, 39, 63.36, 66.05, 67.85, 70 % $CH_4$ recovery and 4.1, 14.3, 14.5, 22.4, 22.5 $mol_{CH_4}.kg_{ads}^{-1}.h^{-1}$ productivity at CSS for, respectively, the 4-step cycle, the 6-step cycle, the 8-step cycle, the 6-step VPSA cycle and, lastly, the optimized 8-step VPSA cycle.

**Keywords :** Pressure Swing Adsorption (PSA), Nitrogen rejection, Biogas upgrading, Aspen Adsorption, Carbon molecular sieve

# Resumo

Esta dissertação foca-se no desenvolvimento de um conceito tecnológico para a remoção de azoto do biogás proveniente de aterros, com uma composição média de 80% de $CH_4$ e 20% de $N_2$. Esta tecnologia terá que ser capaz de gerar um bio-metano com elevada pureza (>97%) e recuperação (>96%). A tecnologia de adsorção, com recurso a uma unidade de *Pressure Swing Adsorption*, foi seleccionada para efetuar esta separação, por salientar-se como um processo maturo, económico e eficiente com uma enorme margem de progresso. Adicionalmente, o adsorvente utilizado neste processo foi um adsorvente do tipo peneira molecular, CMS-3K 172, cineticamente seletivo para o azoto. No entanto, foram realizados estudos preliminares com o adsorvente de carvão ativado, Norit RB-3, seletivo no equilíbrio para o metano. As vantagens de ambos os adsorventes são a sua disponibilidade comercial e o seu custo plausível. Todavia, o uso da peneira molecular como adsorvente é desejável uma vez que a recompressão do produto é desnecessária. Dados de equilíbrio e de cinética foram estudados para ambos os adsorventes e ajustados com o modelo de Langmuir.

O *software* Aspen Adsorption foi utilizado para simular o comportamento dinâmico da adsorção multi-componente num PSA para a qual foi desenvolvido um modelo matemático capaz de o prever, fielmente. Este modelo foi aplicado ao estudo preliminar de componente puro e multi-componente em curvas de *breakthrough* para uma única coluna e também ao desenvolvimento e otimização do comportamento de duas colunas de PSA em ciclos com 4 passos, 6 passos, 8 passos e em processos de PSA com uso de vácuo (VPSA) com 6 e 8 passos.

Os resultados das curvas de *breakthrough* prevêem com veracidade a *performance* de ambos os adsorventes para os quais uma primeira estimativa das dimensões do leito foi realizada através da relação entre a velocidade mínima de fluidização, calculada através da equação de Ergun, e a velocidade intersticial do leito. Foi realizado um estudo paramétrico para compreender a influência de vários parâmetros operacionais num PSA com 4 passos para o qual se concluiu que a performance máxima é atingida ao variar o coeficiente CV da válvula que se encontra na corrente de saída do produto e também o rácio entre a velocidade intersticial do leito e a velocidade mínima de fluidização. Baseado neste estudo, um ciclo com 6 passos por introdução do passo de equalização de pressão e outro com 8 passos por introdução do passo de equalização de pressão e do passo de despressurização co-corrente para os processos de PSA e VPSA foram otimizados com base no critério de fixar a pureza de $CH_4$ a 97% e melhorar a sua recuperação.

Os resultados obtidos foram 97, 97.15, 96.97, 96.92 and 97% de pureza de $CH_4$, 39, 63.36, 66.05, 67.85, 70% de recuperação de $CH_4$ e 4.1, 14.3, 14.5, 22.4, 22.5 $mol_{CH_4}.kg_{ads}^{-1}.h^{-1}$ de

produtividade, obtidas em estado estacionário, para respetivamente, o ciclo de PSA com 4 passos, 6 passos, 8 passos e o ciclo de VPSA com 6 e 8 passos.

**Palavras-chave :** *Pressure Swing Adsorption* (PSA), Rejeição de azoto, *Upgrading* do biogás, *Aspen Adsorption*, Peneira molecular

# Declaration

I hereby declare, under word of honour, that this work is original and that all non-original contributions is indicated and due reference is given to the author and source

*Sign and date*

Sofia Sousa

*March 17th, 2021*

# Index

# List of Figures

# List of Tables

# Notation and Glossary

| | | |
|---|---|---|
| $A$ | Area | $m^2$ |
| $b$ | Adsorption constant for a specific temperature | $bar^{-1}$ |
| $b_0$ | Adsorption constant at infinite temperature | $bar^{-1}$ |
| $c$ | Concentration | $kmol.m^{-3}$ |
| $C_g$ | Gas phase concentration | $kmol.m^{-3}$ |
| $C_{ps}$ | Adsorbent specific heat capacity | $J.kg^{-1}.K^{-1}$ |
| $C_{pw}$ | Wall Material heat capacity | $J.kg^{-1}.K^{-1}$ |
| $D_c$ | Diffusivity coefficient in the adsorbent pores | $m^2.s^{-1}$ |
| $D_L$ | Axial dispersion coefficient | $m^2.s^{-1}$ |
| $d_p$ | Particle diameter | m |
| $F$ | Flowrate | $Nm^3.h^{-1}$ |
| $g$ | Gravitational accelaration | m2.s-1 |
| $H_{amb}$ | Wall/Environment heat transfer coeffient | $MW.m^{-2}.k^{-1}$ |
| $H_w$ | Fluid/Wall heat transfer coeffient | $MW.m^{-2}.k^{-1}$ |
| $IP1$ | 1st Extended Langmuir 2 parameter | $kmol.bar^{-1}.kg^{-1}$ |
| $IP2$ | 2nd Extended Langmuir 2 parameter | K |
| $IP3$ | 3rd Extended Langmuir 2 parameter | $bar^{-1}$ |
| $IP4$ | 4th Extended Langmuir 2 parameter | K |
| $K$ | Henry constant | - |
| $k_{LDF}$ | LDF mass transfer coefficient | $s^{-1}$ |
| $k_w$ | Wall thermal conductivity | $MW.m^{-1}.K^{-1}$ |
| $L$ | Column lenght | m |
| $M$ | Molecular weight of the gas mixture | $g.mol^{-1}$ |
| $m_{ads}$ | Adsorbent mass used in the adsorption bed | kg |
| $n$ | Molar amount | kmol |
| $N$ | Number of nodes | - |
| $P$ | Pressure | bar |
| $P_F$ | Feed pressure | bar |
| $P_L$ | Low pressure | bar |
| $q$ | Equilibrium adsorption capacity | $kmol.kg^{-1}$ |
| $Q$ | Adsorbed amount at infinite pressure | $kmol.kg^{-1}$ |
| $R$ | Universal gas constant | $L.atm.K^{-1}.mol^{-1}$ |
| $RMSE$ | Residual root mean squared error | $kmol.kg^{-1}$ |
| $r_p$ | Particle radius | m |
| $SP_{ij,}$ | Separation Power | - |
| $t$ | Time | s |
| $T$ | Temperature | K |
| $T_{amb}$ | Environmental temperature | K |
| $t_b$ | Breakthrough time | s |
| $t_{cycle}$ | Cycle time | s |
| $t_{diff}$ | Diffusion time | s |
| $T_g$ | Gas temperature | K |
| $t_{st}$ | Stoichiometric time | s |
| $U_i$ | Interstitial gas velocity | $m.s^{-1}$ |
| $U_{mf}$ | Minimum fluidization velocity | $m.s^{-1}$ |
| $U_s$ | Superficial gas velocity | $m.s^{-1}$ |
| $V$ | Bed volume | $m^3$ |
| $y$ | Mole fraction | kmol/kmol |

*Greek Letters*

| | | |
|---|---|---|
| $\alpha_{i,j}$ | Equilibrium selectivity | - |

| | | |
|---|---|---|
| $\alpha'_{i,j}$ | Inherent equilibrium selectivity of a separation | - |
| $\beta_{i,j}$ | Kinetic selectivity | - |
| $\Delta H$ | Adsorption enthalpy | J.kmol$^{-1}$ |
| $\varepsilon_i$ | Inter-particle porosity | - |
| $\varepsilon_p$ | Intra-particle porosity | - |
| $\varepsilon_t$ | Total voidage | - |
| $\mu_g$ | gas mixture viscosity | cP |
| $\xi_m$ | Column mass capacity factor | - |
| $\rho_{ap}$ | Apparent density | kg.m$^{-3}$ |
| $\rho_b$ | Bulk density | kg.m$^{-3}$ |
| $\rho_w$ | Wall density | kg.m$^{-3}$ |
| $t$ | Residence time | s |
| $\varphi_p$ | Shape factor | |

### *List of Acronyms*

| | |
|---|---|
| CMG | Coal Mine Gas |
| CMS | Carbon Molecular Sieve |
| CSS | Cyclic Steady State |
| CV | Valve coefficient |
| DR PSA | Dual Reflux Pressure Swing Adsorption |
| ETS | Engelhard Titanosilicates |
| GHG | *Greenhouse Gas* |
| GWP | *Global Warming Potential* |
| LDF | *Linear Driving Force* |
| LNG | Liquefied Natural Gas |
| LUB | Unused bed |
| MIL | Materials of Institut Lavoisier |
| MOF | Metal Organic Frameworks |
| MSC | Molecular Sieving carbons |
| MTZ | Mass Transfer Zone |
| NG | Natural gas |
| PSA | Pressure Swing Adsorption |
| RNG | Renewable Natural Gas |
| TSA | Temperature Swing Adsorption |
| VOC | Volatile organic components |

# 1 Introduction

## 1.1 Framing and presentation of the work

The world demand for energy is increasing in an environment of unstable energy prices since the conventional fuels which play central roles in our energy supply such as oil and gas are controlled by only a few supplier countries around the world. Climate change and the scarcity of such resources are two of the big challenges the world will face in the near future. In order to counterbalance the current tendencies and guarantee a viable energetic and economical future, action must be taken to deliver sustainable, decentralized and secure energy. In such a way, the development of renewable energy sources is further motivated by the urge to mitigate climate change. To address this matter, the most important global agreement to date, the Paris Agreement, was set into motion, demanding for the countries to set emissions-reduction pledges [1]. Hence, the biogas and biomethane industries play a fundamental role in achieving this goal. Biomethane, upgraded from biogas, is a renewable substitute for natural gas. This alternative displays a diversified range of sources such as landfills, sewage treatment plants and the food industry. The landfill biogas consists, essentially, of methane, carbon dioxide and nitrogen and is widely applicable, either in cogeneration systems, as a source of heat and electricity or, if upgraded to biomethane, it can be directly injected into the gas grid and, if liquefied, used as vehicle fuel, according to the local requirements [2].

The scope of this work will be limited to the separation of nitrogen and methane, a particularly challenging separation due to the resemblance between the two molecules' chemical and physical properties [3]. After an extensive review of emerging and conventional technologies able to perform this selection, the Pressure Swing Adsorption (PSA) technology was selected due to its ability to meet the constraints of this problem as an economical, energy efficient and safe process. Following this, the adsorbent was selected and its adsorption equilibria and kinetics was studied. This preliminary study culminated in the simulation of a PSA system able to remove the nitrogen, by designing the adsorption column, followed by a dynamic analysis, stipulation of the cycle steps and duration and further optimization.

## 1.2 Presentation of the company

DMT Environmental Technology began its journey in 1987 when it was founded by Rob Dirkse to meet the new legislation regarding environmental protection in the late 80's. In 2001, Rob Dirkse's son, Erwin Dirkse took on his father legacy and placed DMT as a strategic competitor in the biogas upgrading market by developing a membrane system able to effectively upgrade biogas to biomethane (CarborexMS). Also, the company developed systems for the

desulphurization of the biogas (Sulfurex), for water treatment (TurboTec) and soil remediation. Nowadays, DMT employs over 70 people, has partnerships with research institutes and Universities and delivers high-performance technologies to be used in the biogas upgrading field. DMT is a company that challenges itself every day to produce green environmental solutions for a sustainable future.

## 1.3 Contribution of the author to the work

To get acquainted with the topic, over 70 journal articles regarding the separation of $N_2$ from $CH_4$ were screened and the most relevant were summarized. In the second phase, the technology able to efficiently execute the separation was chosen which was followed by a methodical choice of the adsorbent, based on its commercial availability, cost and performance. Afterwards, adsorption equilibria and kinetic studies were done which allowed beginning the simulations with Aspen Adsorption, after a period of training. These simulations were progressively optimized by either changing the operating parameters or adding steps in order to deliver the desired end-product. Unfortunately, the end-product that was obtained does not meet all the specified requirements but the right track is being followed towards it.

With the development of this dissertation, DMT Environmental Technology gained a deeper insight of Pressure Swing Adsorption technology, of the different adsorbents able to perform this separation and its challenges. The work done will accelerate the future design and implementation of a PSA unit able to effectively remove nitrogen from biogas and to deliver bio-methane with the required specifications.

## 1.4 Organization of the dissertation

The present dissertation is divided into five different sections:

- **Chapter 2 - Context and state of the art:** Within this section the reason why this separation is challenging and the technologies and adsorbents able to perform it are described as well as some fundamental concepts of adsorption and PSA technology.
- **Chapter 3 - Technical description:** In this chapter a description of the biogas specifications and bio-methane requirements, the selection of the technology and the adsorbent as well as its characterization is given. Also, an overview of the Aspen Adsorption software is presented along with the mathematical model behind the simulations. Additionally, the logic behind the design of the industrial-scale PSA unit is clarified.
- **Chapter 4 - Results and discussion:** The main results obtained during the development and optimization of the PSA unit are addressed in this chapter.
- **Chapter 5 - Conclusion:** An overall review of the entire work is presented.
- **Chapter 6 - Assessment of the work done:** A final review of the developed project is given.

# 2 Context and State of the art

## 2.1 Biogas and bio-methane

Nowadays, the awareness of the impact of greenhouse gases emissions has increased, resulting in many countries declaring a state of 'climate urgency' and committing to reduce their environmental footprint through the research and development of renewable energies. As a result, biogas and biomethane industries have risen as a crucial energy for the much-needed energetic transition to renewables, in part, because of their reliability and availability. The main component in biogas is methane, which is why it has such a high energetic value. Also, this component presents an estimated GWP (Global Warming Potential) of 28-36 over 100 years [4]. Biomethane is upgraded from biogas and thus, a direct response to the reduction of GHG (Greenhouse Gas) emissions by harvesting the methane that would otherwise be released into the atmosphere due to the decomposition of organic waste when sourced from landfills, food and agricultural industries or water treatment facilities [5].

The production of biogas from organic matter - anaerobic digestion - is defined by four steps: hydrolysis, acidogenesis, acetogenesis and methanogenesis [6]. This process can either occur in controlled reactors (bio-digesters) or natural landfills designed for the harvest of this gas, operating at psychrophilic conditions (285-290 K and 1 atm) [7]. In figure 1, a schematic of the anaerobic digestion and all the versatile applications of biogas are represented.

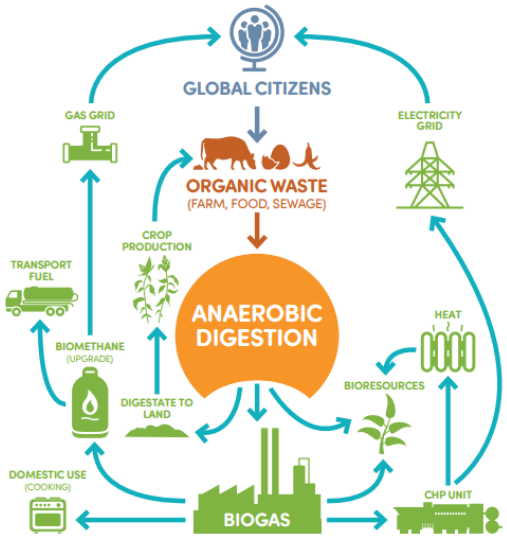


*Figure 1. Anaerobic digestion process as well as biogas applications [5].*

The landfill gas recovery systems are usually covered with a plastic sheet while extraction wells with compressors are used to induce the flow of the produced biogas to a central collection point. However, since these sites are usually not 100 % sealed, air is also introduced in this biogas flow. This situation inevitably results in a nitrogen content in the biogas stream

too high to be used as a natural gas replacement. The table 1 in Appendix A compares the biogas composition from different sources with the natural gas pipeline requirements in both USA and the Netherlands.

In the United States, the production of biogas from landfills accounts for 90% of its total biogas production which was 372 TWh in 2020 [8]. Nowadays, they are world leaders in the development of the biomethane as a transport fuel by liquefaction as a result of state and federal incentive. Since landfill gas composition is very much source dependent, each bio-methane production plant must be adapted to treat the changing inlet flow according to the local/governmental pipeline or liquefied natural gas (LNG) specifications. Although there are local examples of injection of biomethane into the natural gas grid in the USA and Canada, no national standards have been established. Nonetheless, in North America efforts are being made to create a unique quality requirement for the natural gas grid which will normalize and enhance the injection of biomethane in the distribution system [9].

As seen in Appendix A, the quality of the biogas usually does not meet the governmental pipeline specifications. The presence of impurities such as carbon dioxide and nitrogen decrease the calorific value of the renewable natural gas (RNG) [10]. Furthermore, when considering the production of LNG, nitrogen must be removed for three reasons: it is an inert gas with no heating value; its presence demands a much higher energy consumption for the liquefaction of the RNG to occur, larger vessels and larger sizes of the low-temperature equipment; a content of nitrogen in the LNG containers higher than 1% jeopardizes the safety of the process [11]. At the moment, one of the most pressing challenges in the field of landfill biogas upgrading is the nitrogen rejection. Therefore, specific removal technologies must be developed to upgrade the biogas.

## 2.2 The challenges of separating nitrogen and methane

Separation technologies are designed to take advantage of the different physical, chemical or transport properties of the different components in the mixture. The efficiency of the process depends on the difference between these properties. In Appendix B, the components chemical and physical properties are represented.

Regarding physical properties, nitrogen and methane display rather similar ones. Although, a significant disparity exists in their normal boiling point which may suggest that a distillation process could be the solution for this problem. Both molecules are non-polar since they do not exhibit an overall dipole moment, thus their solubilities in common polar solvers are low, although methane presents a higher solubility for organic solvents than nitrogen [12].

As for the molecules' kinetic diameter, it allows to evaluate the possibility of an adsorbate molecule to collide with one of the pore mouths of a certain adsorbent. As both molecules

display a similar kinetic diameter, this limits the possibility of separating them based only on this property. Additionally, similar size molecules might display a different rate of diffusion into the pores due to their surface interactions, hence, allowing the separation [13].

Concerning the chemical properties, some differences may be appointed either because methane can be converted to other chemicals in reactions where nitrogen is inert or since nitrogen can be fixed under the appropriate conditions while methane remains inactive. A brief description of the emerging technologies that exploit these differences is given in Appendix C.

## 2.3 A review of conventional $N_2$ removal from biogas technologies

There are several technologies with the potential to efficiently separate nitrogen and methane. Here, they will be presented, analyzed according to the following criteria: the feed flowrate, energy efficiency of the process, investment and operational costs and also the safety standards.

Since not only the biogas is received at high pressure but also the natural gas is transported at high pressure, it would be advantageous that the resulting biomethane product could be kept at high pressure. To do so, the technology should be nitrogen selective. Since for methane selective technologies, additional energy would be required to depressurize and pressurize the methane gas, resulting in additional steps and higher operating costs. The ideal technology must also meet safety requirement and operate at moderate temperature and pressure, so that it would be easily adaptable to current industrial processing plants.

### 2.3.1 Cryogenic Distillation

Nowadays, this well-known separation process is the only to have reported for nitrogen removal at gas flows above 28 000 $Nm^3.h^{-1}$, a recovery of 98% and purity of 99% for $CH_4$. Cryogenic distillation relies on the different volatilities of the mixture and must operate under cryogenic conditions which demands a pre-treatment for the separation of $CO_2$, additional capital costs with the cryogenic equipment and extremely high operating costs due to the need of $N_2$ liquefaction [11].

The high energy requirements and operational/capital costs result in a less attractive technology, specifically for small-scale applications. This technology is well suited for large natural gas reservoirs which can be exploited for about 20 years delivering up to 500 000 $Nm^3.h^{-1}$ [14] or even for LNG production, but only if the flow rate is higher than 17 000 $Nm^3.h^{-1}$[12].It is estimated that in order to process biogas streams smaller than 1100 $Nm^3.h^{-1}$, the relative cost per $Nm^3$ of RNG produced becomes 3 times more expensive when comparing it with a plant capacity of 20 000 $Nm^3.h^{-1}$ [15].

### 2.3.2 Membranes

A membrane behaviour is similar to that of a semi-permeable barrier since it remains impermeable for certain components of a mixture when exposed to the action of driving forces such as the different partial pressures or a chemical potential gradient between both sides of the membrane. This technology displays several improvements over some traditional processes as cryogenic distillation and gas-liquid absorption since no phase change is required, it operates at moderate temperatures, it is easily adapted for remote and unmanned sites and presents low capital and operating costs [12]. A thorough analysis of the different membrane types is presented in Appendix D. In review, although the membrane technology offers a promising alternative for being scalable, safe and energy efficient (for nitrogen selective membranes), advancements must be done on their manufacturing process to obtain membranes with competitive separation performances.

### 2.3.3 Absorption

This separation process is a mature and widely applied one, which uses a liquid solution to separate a gas mixture in an absorption tower, while absorbing the component with the highest solubility. The absorbate is then regenerated in a stripper either by staged pressure reduction or thermally driven distillation [11]. An example of a $CH_4$ selective process uses a lean oil solvent and processes 2000 to 30 000 $Nm^3.h^{-1}$ of biogas, while obtaining a purity of 96% of $CH_4$ [12]. Nonetheless this technology is not well-adapted for the removal of nitrogen in natural gas plants since there is a deficiency of proper liquid solutions that while being selective either for methane or nitrogen also meet the economical and safety factor.

### 2.3.4 Adsorption

Adsorption is defined as a spontaneous attraction occurrence between a molecule from a fluid phase, the adsorbate, and the porous surface of a solid, known as the adsorbent [16]. Adsorbents are porous solids which demonstrate a large surface area per unit mass with a range of micropores and macropores which are usually interconnected to form a pore network. Both physical and chemical properties of the adsorbent determine the selectivity towards a certain adsorbate. In adsorption processes, the adsorbent is well-compacted inside a fixed bed column, where the process occurs.

The separation of gas mixtures by the selective adsorption of a certain component is a well-stablished technology and dominant when it comes to air purification [17], production of hydrogen [18] and the removal of $CO_2$ from the combustion exhaust gas produced in power plants [19]. Within the NG and RNG processing industries, technologies based on adsorption have been gaining leverage due to the promising reduced capital and operating costs while delivering high separation performances, when compared with traditional technologies [20].

Adsorption processes can be classified according to the method employed to regenerate the adsorbents into two main categories: Temperature Swing Adsorption (TSA) and Pressure Swing Adsorption (PSA). However, TSA process is not a valid option for the separation of $N_2$ and $CH_4$ due to the relatively weak sorption strength of both components on most adsorbents.

In contrast to TSA, PSA operates quickly due to the relatively easy cycle alternation between pressurization and depressurization, resulting in higher productivities. The only energy required for the PSA process is in the form of compression work. Moreover, if the strongly adsorbed component is not required at high pressure, there is even no need for recompression. PSA process emerges as a promising energy efficient technology to meet the constraints of this process.

Generally, these processes fit smaller scale gas processing facilities (<16 000 $Nm^3.h^{-1}$) which perfectly suits the separation in question. Furthermore, PSA offers the possibility to separate nitrogen from methane and ticks all the presented criteria. The only current obstacle is the development of a proper adsorbent. Further research must be focused on possible adjustments to the PSA process design and also on adsorbent's enhanced performance, cost and reliability.

In the following chapters the fundamental concepts of adsorption, the main obstacles that PSA technology faces to achieve high performance selectivites for this specific separation and some possible modifications to the fundamental Skarstrom cycle will be presented.

## 2.4 Fundamental concepts of adsorption

In adsorption processes, in terms of energy efficiency, it is better to remove the minor component in a feed mixture. Hence, it is expected that using a nitrogen selective adsorbent for landfill gas upgrading will favour the process economics of PSA units [21]. This selectivity phenomena to a certain component in a gas mixture might be achieved either by one or a combination of the following methods [22]:

1. Differences in the adsorbate-surface interactions and/or adsorbate packing interactions when the system reaches the equilibrium (thermodynamic equilibrium mechanism);
2. Differences in the size and/or shape of gas molecules leading to the exclusion of molecules with a larger critical diameter so that they cannot penetrate the adsorbent pores (steric mechanism);
3. Differences in the diffusion rates of molecules through the adsorbent pores (kinetic mechanism).

Hence, it is possible to distinguish two types of adsorbate selectivity:

1. Equilibrium selectivity which is achieved in the limit of long time periods. It can be translated as $\alpha_{i,j}$:

$$\alpha_{i,j} = \frac{q_i/y_i}{q_j/y_j} \quad as \quad y_i, y_j \to 0 \tag{1}$$

where $q_i$ and $q_j$ are the equilibrium adsorption capacities determined from pure gas component isotherms and $y_i$ and $y_j$ are the mole fractions of the components in the gas mixture. Moreover, the separation factor might be estimated by the ratio of the Henry's constants $\left(K_i/K_i\right)$. Also, the working capacity is an important parameter which, regarding PSA, is the difference between the uptake/capacity at the feed pressure and regeneration pressure [23]. This factor is related to the shape and magnitude of the adsorbent's isotherm and is given by $n_{ads}$-$n_{des}$, according to Figure 2.

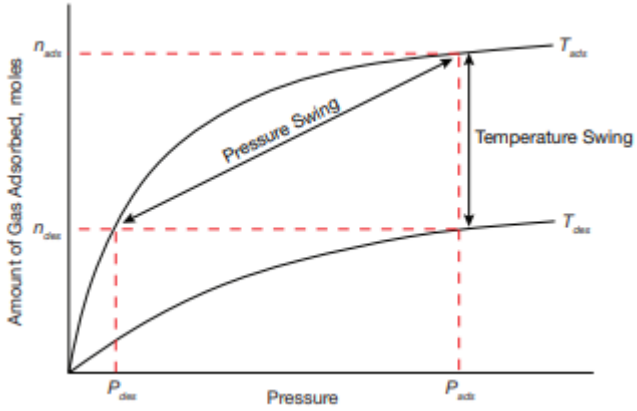


*Figure 2. Isotherm of an adsorbent with indications for the determination of its working capacity, for both PSA and TSA processes.*

Consequently, both product purity and recovery are limited by the nominal pressure ratio in the adsorbent column [24]. Although, this situation can be surmounted with a recycling of the purified product(s) to the beds to increase the local pressure of certain gases [25].

2. Kinetic selectivity which is time dependent selectivity. This selectivity considers the diffusivity ratio (assuming $k_i \propto D_{c,i}$ where the last represents the diffusivity coefficient of component $i$ in adsorbent pores) and the equilibrium selectivity. So, an overall selectivity takes place:

$$\beta_{i,j} = \alpha_{i,j}\sqrt{\frac{k_i}{kj}} \tag{2}$$

Where $k_i$ and $k_j$ accounts for each component's sorption mass transfer coefficient.

### 2.4.1 Adsorbents

Currently, there are no commercially available adsorbents displaying an equilibrium selectivity for nitrogen over methane, although some metal organic frameworks (MOFs), which are still under study, have been reported [26]. On the other hand, there are accessible

adsorbents at an industrial scale which exhibit selectivity based on molecular sieving effects and/or the different diffusivities of $N_2$ [21]. Moreover, adsorption processes based either on the equilibrium adsorption of $CH_4$ using activated carbons or the adsorption of $N_2$ using narrow pore adsorbents such as titanosilicates have already been demonstrated for the upgrading of high $N_2$ content natural gas reservoirs [27, 28].

As mentioned before, preferably, the process should be nitrogen selective in order to keep the energy costs at a minimum. The following adsorbents are all nitrogen selective except for an activated carbon, the Norit-RB 3.

#### 2.4.1.1 Carbon Molecular Sieves

Carbon molecular sieves (CMS), also known as molecular sieving carbons (MSC), are a category of activated carbons with a porous composition usually with a width shorter than 20 Å [11]. This width is often similar to one of the adsorbate molecules, inducing a significant number of collisions between the molecules and the pore mouths. In addition, similar size molecules often display a different rate of diffusion into the pores due to their different surface interactions [13].

Due to the similar kinetic diameter of the molecules, a separation based on the different diffusion rates and the molecular sieving effects in the adsorbent's pores requires a well-controlled, narrow pore size distribution. This kind of adsorbent does not show a significant equilibrium capacity for nitrogen or methane as that of activated carbon or zeolites but, on the other hand, it offers a considerable kinetic selectivity for nitrogen over methane [29]. For the adsorbent MSC-3K-172, a commercially available adsorbent, G.Xiao et al. simulation work reported for a biogas feed with 75% $CH_4$ and 25% $N_2$ a purity and recovery of 90%, under the implementation of the Dual Reflux Pressure Swing Adsorption Process (DR PSA), a cycle modification which is explored in Appendix E [21].

#### 2.4.1.2 Zeolites

This type of adsorbent is a crystalline aluminosilicate with a well-defined and uniform microporous structure, with a pore's size comprehended between 3 to 11 Å [30]. Its adsorption characteristic is due to its porous structure which enables smaller molecules insertion, adsorbing them. Different zeolites, with different characteristics and pore's size, can be obtained by varying either the temperature, pressure or pH during its manufacturing, the sources of aluminium and silicon and also the number or the type of cations ($Na^+$, $Li^+$, $K^+$ or $Ca^{2+}$) in its extra-framework structure [31].

Zeolites have effectively been used in natural gas upgrading for the removal of nitrogen. Most of them are recognized for being methane selective based on thermodynamic equilibrium and may exhibit an equilibrium selectivity of methane over nitrogen of 3 to 4. However, certain

zeolites may also present much larger adsorption kinetic rates for nitrogen over methane, and results comparable to those obtained with titanosilicates, which would be beneficial for landfill gas processing [11].

#### 2.4.1.3 Titanosilicates

Engelhard titanosilicates (ETS) are materials containing $Ti^{+4}$ and $Si^{+4}$ in octahedral and tetrahedral coordination, respectively [32]. Over the last 25 years, Engelhard Corp. has developed and patented a family of titanium silicate ($aNa_2O:bTiO_2:ySiO_2:zH_2O$) molecular sieves and has named them ETS-4, ETS-10, and ETS-14. Engelhard Titanosilicate-4 (ETS-4) is, industrially, the most significative molecular sieving adsorbent for the capture of nitrogen from methane and has been used in commercial natural gas upgrading applications [33, 34]. This adsorbent has demonstrated an accurate tunable micropore size comprehended between 3 and 4 Å as seen in Figure 3 [35]. This technology is commercially known as Molecular Gate® process, while being provided by BASF SE and offered as modular plants by Guild Associates, therefore, they cannot be commercialized by any other parties [35]. A drawback of this technology is its lack of robustness when faced with thermal activation [21].

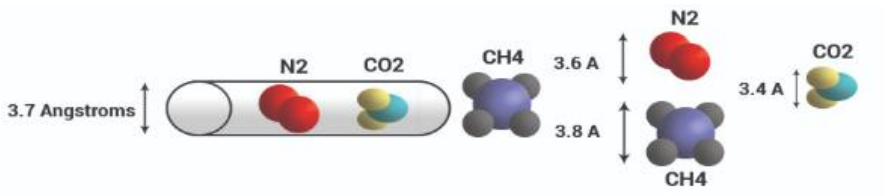


*Figure 3. Comparison between the molecular diameters of $CH_4$, $N_2$, $CO_2$ and the micropore size of the adsorbent [36].*

Overall, the advantages of adsorbing with titanosilicates are low energy consumption, flexible operation and an inexpensive operation compared to other gas separation processes, which can produce up to 99% pure streams as well as high recoveries lead to an effective application in separation processes [32].

#### 2.4.1.4 Metal organic frameworks

Titanium silicates and carbon molecular sieves like the previously described ETS-4 and MSC-3K-172 are rare examples of porous materials able to effectively separate nitrogen from methane kinetically. Nonetheless, as previously stated, as they present a considerable kinetic selectivity, it lacks in equilibrium selectivity, downgrading the overall quality of the separation [37].

Hence, the design of a porous solid that combines a high equilibrium selectivity for $N_2$ over $CH_4$, a large $N_2$ uptake and easy regeneration is highly challenging for separation-based technologies. Such a porous solid would have to contain unsaturated transition metal sites to

strongly bind the nitrogen at equilibrium – MOF's - due to easy control of the reactivity and concentration of these sites. Recently developed numerous kinds of zinc-based metal-organic frameworks (MOF) are considered to be ideal adsorbents owing to their very high specific surface area, tunable pore size and large accessible pore volume, although they are not commercially available and some haven't even been synthesized. In this context, the institution Lavoisier developed a series of mesoporous metal (III) trimesate MIL-100(M) (MIL: Materials of Institut Lavoisier) containing a large concentration of chemically tunable unsaturated metal sites (M = Al, Cr or Fe). The MIL-100-Cr was proven to be the first-ever adsorbent able to thermodynamically capture nitrogen over methane and oxygen with large $N_2$ uptake and easy regeneration [26].

#### 2.4.1.5 Activated Carbon

The extra cost of recompression when using adsorbents selective for $CH_4$ might be overlooked if the composition requirements of pipeline gas are fulfilled by the nitrogen removal by selective adsorption on $CH_4$. Activated carbons are produced from the anaerobic pyrolysis of carbonaceous materials. The commercially available Norit-RB 3 is equilibrium selective for methane, and, similarly to the mentioned CMS, although it presents a low overall selectivity, there is room for improvement with the implementation of a Dual Reflux PSA, for example [24].

### 2.4.2 The challenge behind the capture of nitrogen from landfill gas with PSA technology

Related to the PSA functioning, a feed stream enters a bed packed with adsorbent particles (adsorption or feed step) selective to the heavy (more adsorbed) component, while the light component (less adsorbed) is obtained at the top of the column at operation pressure.

The adsorber phase displays a concentration gradient from zero to equilibrium known as mass transfer zone (MTZ) - where the adsorption occurs. This step is discontinued before the MTZ front reaches the top of the column to prevent the adsorbent's saturation within the column and resultant product contamination. Subsequently, the column undergoes a depressurization step which regenerates the column by the desorption of the impurities – depressurization or blowdown step. The regeneration is enhanced by a purge with the light component - purge step. Lastly, the column is partially pressurized with the feed stream and is now ready to restart the cycle - pressurization step. At first, a higher product flow used as purge should enhance the process purity since the heavier component is being more effectively removed. Nonetheless, the system recovery diminishes since the end-product is being wasted in the purge flow. This situation perfectly represents the compromise that prevails between the purity and recovery of the PSA unit while optimizing it [38].

These four cyclic steps are known as the Skarstrom cycle and represent the foundation base of a PSA, which can be operated with two beds where the adsorption/purge and

pressurization/depressurization steps always work in pairs and indicate that, for example, while one of the beds is pressurizing, the other is depressurizing in every half cycle. An adapted scheme of the two column PSA introduced by Skarstrom in 1960 is represented in figure 4.

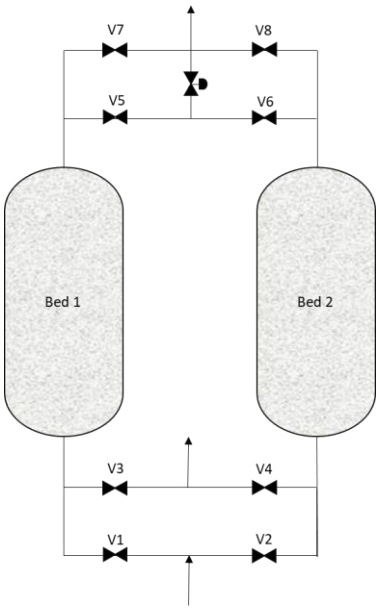


| | | | | |
|---|---|---|---|---|
| **Bed 1** | **Adsorption** | **Depressurization** | **Purge** | **Pressurization** |
| | V1, V7 | V3 | V5,V3 | V1 |
| **Bed 2** | **Purge** | **Pressurization** | **Adsorption** | **Depressurization** |
| | V6,V4 | V2 | V2,V8 | V4 |

*Figure 4. 2-column PSA scheme and valve sequencing for the steps in Skarstrom cycle. Adapted from [39].*

### 2.4.3 Skarstrom modifications

#### 2.4.3.1 Vacuum Pressure Swing Adsorption

Despite of the Skarstrom cycle ability to produce a primary product with high purity, it usually fails to achieve a reasonable enrichment. To address this matter, it is common to operate the purge step under vacuum conditions towards intensifying the pressure difference. This process is called Vacuum Pressure Swing Adsorption (VPSA) and delivers an optimized performance and productivity alongside a higher energy consumption when the purpose is to recover methane from its low concentration sources such as Coal Mine Gas (CMG). However, VPSA might not be suitable for an economical recovery of methane from high grade sources [40].

#### 2.4.3.2 Pressure equalization step

According to Skarstrom, the column that finishes the adsorption step is depressurized to atmospheric conditions, losing a significative portion of the light component. To enhance the system recovery, the equalization step plays a fundamental part – after the pressurized column goes through adsorption and the other column is purged at low pressure, the connected columns equalize the pressure between them. Thus, the gas that would be otherwise lost in depressurization is used to pressurize the column getting ready for the adsorption step [38]. Other Skarstrom modifications which were not directly explored are represented in Appendix E.

# 3 Technical description

DMT Environmental technology has been working on new and more efficient technologies to upgrade biogas streams, but nitrogen removal to the extent required by natural gas pipelines in the USA for the injection of biomethane requires the development of a new improved system. As mentioned before, biomethane quality standards are not regulated at a federal level, which implies that for each specific biomethane project an agreement of the biomethane standards with gas utility parties must be discussed.

Due to the market opportunity of this separation in the biomethane and LNG sector, DMT-ET is motivated to effectively capture nitrogen from biogas streams while meeting the specifications of the client. Hence, decisions must be considered to select the most well-suited technology for this problem, such as the technology's particularities, the adsorbents, the selected software to simulate it and the chosen model to describe it.

## 3.1 Biogas specifications and biomethane requirements

It is important to mention that the landfill biogas stream that will be used for the purpose of this project must be pre-treated as shown in Figure 5. This process starts with a cooling step followed by a drying step to remove part of the water. This drying step must achieve a dew point below -3ºC to avoid condensation at low temperatures during the blowdown step. Afterwards, an absorption column with either water or sulphuric acid as solvent, in counter-current, is applied to remove the volatile organic components (VOC), hydrogen sulphide, siloxanes and ammonia. This step is usually followed by a membrane system, specifically for this study case, to capture the carbon dioxide. Subsequently, the biogas has the required conditions to enter the PSA unit for bio-methane upgrading.

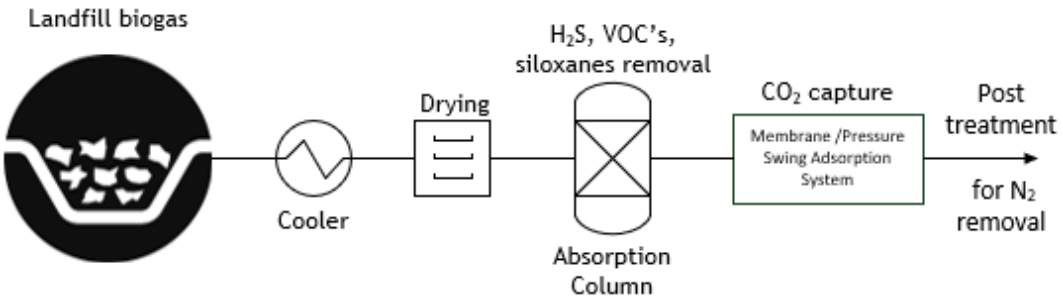


*Figure 5. Schematic of landfill biogas pre-treatment, before nitrogen removal unit.*

Both landfill biogas specifications, after pre-treatment, and the RNG requirements after nitrogen removal received by the R&D department are listed in Table 1.

*Table 1. Landfill biogas characteristics received for nitrogen removal and bio-methane requirements alongside the stablished ranges.*

| | **Biogas Specifications** | | | **Bio-methane requirements** | | |
|---|---|---|---|---|---|---|
| | MIN | MAX | **NOM** | MIN | MAX | **NOM** |
| **Temperature, *T* (K)** | - | - | 298,15 | - | - | 298,15 |
| **Pressure, *P* (bar)** | 11 | 16 | 11 | 9 | 20 | 10 |
| **Dew-point (ºC)** | -60 | -80 | -67 | - | - | - |
| **Flowrate, *F* ($Nm^3.h^{-1}$)** | 300 | 600 | 500 | - | - | - |
| **$CH_4$ Purity (%)** | 90 | 75 | 80 | - | - | >97 |
| **$N_2$ (%)** | 10 | 25 | 20 | - | - | <3 |
| **$CH_4$ Recovery (%)** | - | - | - | - | - | >96 |

## 3.2 Technology Selection

In order to select the proper technology, a comparison table was elaborated in Appendix F, considering the criteria listed earlier in chapter 0 and also two decisive factors, namely, the inherent equilibrium selectivity of a separation ($\alpha'_{i,j}$) which is a property common to all of the processes [41] and the separation power, $SP_{ij,}$which takes into consideration the entire process and the optimization potential that can be achieved through process' modifications such as multi-stage separations [42]. Both properties are described in Appendix F.

Among the discussed conventional technologies, adsorption stands out as a mature, well-established promise for the removal of nitrogen from natural gas, as well as a process with a large margin of progress and optimization. Additionally, it offers the possibility to selectively remove nitrogen over methane, enhancing the energetic efficiency of the process and reducing the operating costs. Its equilibrium selectivity might be low but the kinetic selectivity for nitrogen over methane is reported to be as high as it will be analysed in the following chapter.

## 3.3 Adsorbent Selection and characterization

The adsorbent selection is one of the most important decisions during the project of a PSA unit. The selection of the finest adsorbent for a specific separation lies on five criteria: capacity, selectivity, chemical and mechanical resistance, kinetics, cost and market availability. An extensive research of all the adsorbents reported to be able to separate nitrogen from methane either kinetically or at equilibrium was elaborated where over 40 journal articles were screened. In Appendix G some of the most relevant adsorbents for this

project are compared in terms of their equilibrium selectivity ($\alpha_{i,j}$) and kinetic selectivity ($\beta_{i,j}$) as described, respectively, in equations (1) and (2).

In line with Appendix G, titanosilicates deliver the best selectivities for nitrogen over methane. Nonetheless, ETS adsorbents are patented and, therefore, are not commercially available. Molecular sieve carbon 3K-172 is a robust adsorbent, unlike titanosilicates, and it is widely used in various industries [43]. Although it is $CH_4$ selective at equilibrium, when considering the micropore diffusion of $N_2$, it is sufficiently fast so that it is kinetically selective. Even though its selectivity is moderate when comparing it with other refined adsorbents such as Clinoptilolites, MOF's and titanosilicates, it is widely available at a reasonable price and the PSA cycle can be modified and optimized to meet the green gas standards. Also, the mass transfer coefficient of $N_2$ is about 100 times higher than that of $CH_4$, a considerable value [44].

Furthermore, due to its availability and for a matter of comparison, Norit-RB3, $CH_4$ selective at equilibrium, will be considered.

*Table 2. Adsorbent characterization.*

| | **MSC-3K 172** | | **Norit-RB3** | |
|---|---|---|---|---|
| **Shape** | Cylindrical | | | |
| **Particle diameter, $d_p$ (m)** | 0.001 | [44] | 0.003 | [24] |
| **Shape factor, $\varphi_p$** | 0.832 | [44] | 0.752 | [45] |
| **Inter-particle porosity, $\varepsilon_i$** | 0.33 | [21] | 0.42 | [46] |
| **Intra-particle porosity, $\varepsilon_p$** | 0.46 | [21] | 0.65 | [46] |
| **Bulk density, $\rho_b$ (kg.m$^{-3}$)** | 657.9 | [21] | 750 | [46] |
| **Adsorbent specific heat capacity, $C_{ps}$ (J.kg$^{-1}$.K$^{-1}$)** | 1100 | [21] | 1500 | [46] |

Even though these parameters are important to primarily rank the adsorbents, the adsorption equilibrium of pure fluids and multicomponent systems is crucial to understand the interaction between the adsorbent and the gas mixture. The adsorption isotherm's data for single component $N_2$ and $CH_4$ will be fitted in Chapter 4.1using the Ideal Langmuir model.

The Langmuir model is one of the simplest and most widely applicable isotherms which is based on the following assumptions: the adsorbent surface is energetically homogeneous; the probability of adsorbing is equal for every site; each active site can only accommodate one molecule and this phenomenon does not interfere with adjacent adsorbing sites. This model is well represented by equation (3) as a function of the partial pressure *P* [47]:

$$q = Q\frac{bP}{1+bP} \quad (3)$$

$$b = b_0\left(\frac{-\Delta H}{RT}\right) \quad (4)$$

Here *q* is the adsorption capacity, *Q* is the adsorbed amount at infinite pressure, *b* is the adsorption constant for a specific temperature, $b_0$ is the adsorption constant at infinite temperature, *ΔH* is the adsorption enthalpy, *R* is the universal gas constant and *T* is the temperature.

Within the adsorption technology, the adsorption equilibria of mixtures is usually more interesting due to the different interaction of individual adsorbates when mixed with others with the solid surface of the adsorbent [48]. Therefore, Aspen Adsorption uses the input given by pure equilibrium parameters and predicts mixture equilibrium by including the competition between the adsorbate molecules for the active sites [49].

Hence, equation (3) might be extended to multi-component and adapted to serve as input to Aspen Adsorption software, according to the model Extended Langmuir 2:

$$q_i = \frac{IP_1 e^{\frac{IP_2}{T_g}} P_i}{1+\sum(IP_3 e^{\frac{IP_4}{T_g}} P_j)} \quad (5)$$

To compare the fitted adsorption isotherm ($q_{corr}$) with the experimental ($q_{exp}$) values for all $n$ observations, the residual root mean squared error (RMSE) equation was applied:

$$RMSE = \sqrt{\frac{1}{n-1}\sum(q_{exp}-q_{corr})^2} \quad (6)$$

Small values of RMSE are indicative of a good model approximation [50].

## 3.4 Aspen Adsorption

With the purpose of validating the design and reproducing the behaviour of the PSA unit for the production of biomethane, simulations were made with the software Aspen Adsorption.

### 3.4.1 Building the flowsheet

The software proposes two different simulation modes: the gas Dynamic and gas CSS. While the first is destined for either cyclic or non-cyclic adsorption processes, the gas CSS mode is only adapted to be used when the adsorption process is cyclic. For the purpose of this work, all the simulations were executed according to the gas Dynamic mode.

Within the gas Dynamic package, the adsorption bed is the element which requires more details and specifications, since it is where the actual adsorption phenomenon takes place, which will be analysed in the following sections of this chapter.

This block is usually accompanied by an upper and bottom tank void, two well-mixed tanks which act as pressure setters for the adsorption bed and, therefore, can be configured according to the desired initial volume, molar composition, pressure and temperature [51].

The valves or Gas Valves may display four different configurations: completely closed (0), completely open (1), with a constant CV (2) or with constant flowrate (3). The coefficient CV is the ratio between the flowrate and pressure drop throughout the valve.

Both the inlet and outlet of the process, named as Gas Feed and Gas Product, respectively, can be designed to have the desired molar composition, pressure, temperature and flow rate.

### 3.4.2 Form configuration

Within this window, it is possible to decide the number of layers of the adsorption bed, corresponding to independent beds with their individual set of constant and/or initial values which is useful if, for example, two different adsorbents are packed in the same column.

The selected geometry of the bed was vertical, preventing flow variation along its width, and its spatial dimensions were set as 1D, evaluating the second order derivatives in the axial direction and so, disregarding the radial one.

### 3.4.3 General window

Here, it is possible to choose among the numerical options able to approximate the partial differential equations, also known as the discretization method. The Upward Differencing Scheme 1 (UDS1) option is one of the best standard methods, representing a first-order upwind differencing scheme, founded on a first-order Taylor expansion. Also, the number of axial nodes chosen for this method was 10.

### 3.4.4 Material and momentum balances window

This tab was used to specify the material balance for the bulk gas adsorption, which is generally described by equation (7) for 1D models, consisting of four terms, the axial dispersion contribution, the convection, the gas phase accumulation and the adsorbed phase accumulation, in order of appearance:

$$-D_L \varepsilon_i \frac{\partial^2 C_g}{\partial x^2} + \frac{\partial (U_s C_g)}{\partial x} + \varepsilon_t \frac{\partial C_g}{\partial t} + \rho_b \frac{\partial Q}{\partial t} = 0 \qquad (7)$$

Where $D_L$ represents the axial dispersion coefficient, considered to be constant, $C_g$is the gas phase concentration, $v_s$ is the superficial gas velocity and $\varepsilon_t$ is the total voidage, calculated as follows:

$$\varepsilon_t = \varepsilon_i + \varepsilon_p(1 - \varepsilon_i) \qquad (8)$$

Regarding momentum balances, it was considered that the gas flow through the packed bed is driven by pressure gradients and also that the flow is turbulent, hence the most general

equation – Ergun equation – was chosen to describe it. This equation combines the Blake-Kozeny model, specific for laminar flows and the Burke-Plummer model, for turbulent flows, respectively, in the first and second term of equation (9):

$$\frac{\partial P}{\partial x} = -\left(150\frac{\mu_g(1-\varepsilon_i)^2}{(2r_p\varphi_p)^2\varepsilon_i^3}U_s + 1.75\frac{M\rho_g(1-\varepsilon_i)}{2r_p\varphi_p\varepsilon_i^3}{U_s}^2\right) \quad (9)$$

Here, $\mu_g$ is the gas mixture viscosity, $r_p$ is the particle radius, $M$ is the molecular weight of the gas mixture.

### 3.4.5 Kinetic model window

For a simulation to truthfully describe an adsorption process, a reliable description of the adsorption kinetics for the selected adsorbent must be developed. Hence, it was decided that the mass transfer driving force is expressed as a function of the solid phase loading, instead of the gas phase concentration. For the adsorbate molecules to diffuse into the adsorbent particles, they move through the macropores of the adsorbents into the micropores, where they reach the actual active site where adsorption occurs. The mass transfer resistances verified in this process may occur due to the resistance between the bulk gas phase and the gas-solid interface or to the specific porous structure of the adsorbent, thus, the presence of macropores and/or micropores. Commonly, the controlling mechanism for $N_2$ and $CH_4$ diffusion into Norit RB3 is macropore diffusion, while for CMS-3K 172 is micropore diffusion [44]. Knowing this, a Lumped Resistance model was selected, which allows to lump the different mass transfer resistances into one factor or to consider that the effect of one dominates, disregarding the others. Among the approximations possible to describe this kinetic model, the Linear Driving Force (LDF) was selected since it is widely used and, in comparison with others such as the Fickian Diffusion, it demands a shorter computational time [30]. Its general form for an adsorbate is given by:

$$\frac{\partial q_t}{\partial t} = k_{LDF}\,(q_\infty - q_t) \quad (10)$$

Here, $q_t$ is the molar adsorbed amount of adsorbate at time $t$, $q_\infty$ is the equilibrium gas phase concentration at gas phase pressure *P* and adsorbent temperature *T* and $k_{LDF}$ is the LDF mass transfer coefficient for the equilibrium adsorbed amount ($q_\infty$). The inverse of the LDF constant, for a certain temperature, is the time that the molecules take to reach the active center of the adsorbent ($t_{diff}$).

### 3.4.6 Energy balance window

The energy balances are represented in Appendix H [48].For this project it was assumed that the energy balance is non-isothermal. After evaluating the relevance for this application, the axial thermal conduction terms were neglected for the gas and solid phases, alongside the heat

of adsorbed phase in the solid phase energy balance. Whereas the heat of adsorption in the solid phase was considered constant for each component $i$, the heat transfer coefficient (HTC) was also considered constant as well as the gas/wall heat transfer coefficient and the solid phase heat capacity. To describe the heat transfer to the environment, the wall energy balance was used, also known as rigorous model, where the wall is presumably thin enough but conductive too so that there is no distinction between outer and inner wall.

## 3.5 Industrial-scale PSA design

The separation performance of the designed PSA cycle was progressively evaluated and optimized according to three main factors: purity, recovery and productivity. These are calculated as follows:

$$Purity = \frac{n_{CH_4(product)}}{n_{CH_4(product)} + n_{N_{2(product)}}} \tag{11}$$

$$Recovery = \frac{n_{CH_4(product)}}{n_{CH_4(feed)}} \tag{12}$$

$$Productivity = \frac{n_{CH_4(product)}}{t_{cycle} m_{ads}} \tag{13}$$

Here, $n$ represents the molar amount of either $CH_4$ or $N_2$, $t_{cycle}$ is the cycle duration and $m_{ads}$ is the adsorbent mass within the adsorption beds.

Knowing the inlet gas mixture pressure, temperature, flowrate, composition and density it is possible to approximate the bed dimensions through the following strategy.

It is known that the interstitial velocity ($U_i$) of the packed bed must always be smaller than the minimum fluidization velocity ($U_{mf}$) to guarantee the stability of the adsorbent particles. In a fluidized bed, the fluid applies an equal force, in intensity, to that of the apparent weight ($P_{ap}$) of the bed but in opposite directions, which is translated by the following equation:

$$P_{ap} = (\rho_b - \rho_g) g (1 - \varepsilon_i) A L \tag{14}$$

Where $g$ is the gravitational acceleration and $A$ and $L$ represent the bed area and length. Considering this, the $U_{mf}$ is calculated by the equalization of a general version of Ergun equation (9) for a fixed bed and equation (14):

$$(\rho_b - \rho_g) g (1 - \varepsilon_i) = 150 \frac{(1 - \varepsilon_i)^2}{{\varepsilon_i}^3} \mu_g \frac{U_{mf}}{{\varphi_p}^2 {d_p}^2} + 1{,}75 \frac{(1 - \varepsilon_i)}{{\varepsilon_i}^3} \rho_f \frac{{U_{mf}}^2}{\varphi_p {d_p}^2} \tag{15}$$

Hence, by arbitrating the ratio of $U_i$ to $U_{mf}$ ($U_i/U_{mf}$) between 0 and 1 it is now possible to calculate the cross-sectional area and therefore, the diameter. Moreover, the column length is given by assuming a ratio between the length and the diameter of the column (L/D). To simulate

an ideal plug flow behavior inside the bed (a good flow distribution with insignificant dead volumes), this parameter should be higher than 5 [52]. On the other hand, this also results in a higher pressure drop so that for the design of this PSA it will be kept lower [53]. Another important parameter is the superficial velocity ($U_s$) which is calculated by multiplying $\varepsilon_i$ and $U_i$.

### 3.5.1 Breakthrough curve analysis

A breakthrough curve represents the concentration history of the outlet stream and is often used as a realistic prediction of an adsorbent separation performance. The mass transfer zone (MTZ) incorporates a gradient from zero to equilibrium, where the actual adsorption occurs and travels across the adsorption bed, while the amount of saturated adsorbent increases until the column is completely saturated or exhausted. Throughout this process, two important times occur: the breakthrough ($t_b$) and the stoichiometric time ($t_{st}$). The first corresponds to the time at which the product concentration reaches 5% of the inlet one and should be used as adsorption time since it is when the maximum performance of adsorption is assured. Whereas $t_{st}$ is the theoretical operating time, which is the time required to saturate the column if the axial and other dispersion effects were neglected, resembling a plug flow behavior. Therefore, for favorable adsorption equilibrium isotherms, considering no dispersion effects, the concentration front along the bed would be described by a shock wave. The $t_{st}$ can be predicted by the following equations [54]:

$$t_{st} = (1 + \xi_m)\,\tau \tag{16}$$

$$\xi_m = \left(\frac{1-\varepsilon_i}{\varepsilon_i}\right)\rho_{ap}\,\frac{q_F}{c_F} \tag{17}$$

$$\tau = \varepsilon_i \frac{V}{F} = \frac{L}{U_i} \tag{18}$$

Where $\xi_m$ is the column mass capacity factor, $\tau$ is the time than a non-adsorbed component takes to cross an adsorption bed, $q_F$ is the adsorbed concentration in equilibrium with $c_F$, the inlet feed concentration. Furthermore, the simple Length of Unused bed (LUB) method allows the design and scale-up of a PSA apparatus and is defined as follows [53]:

$$LUB = \left(1 - \frac{t_b}{t_{st}}\right)L \tag{19}$$

# 4 Results and discussion

## 4.1 Adsorption equilibria and kinetics

The adsorption isotherm's data for single component $N_2$ and $CH_4$ for Norit RB-3 was measured with a dynamic breakthrough method, which has the advantage of a higher operating pressure range, and was extracted from Saleman et al. (2017) [29]. However, for CMS-3K 172 the measured data was obtained from Xiao et al. (2019) [21] with the traditional volumetric method. Since this adsorbent presents such low kinetics for $CH_4$ it was not possible to find measured isotherm data covering the pressure range that will be used in this project. The measured adsorption isotherms were regressed using the Langmuir model as seen in Figure 6 where the correlated curves are plotted alongside the experimental data for comparison purposes.

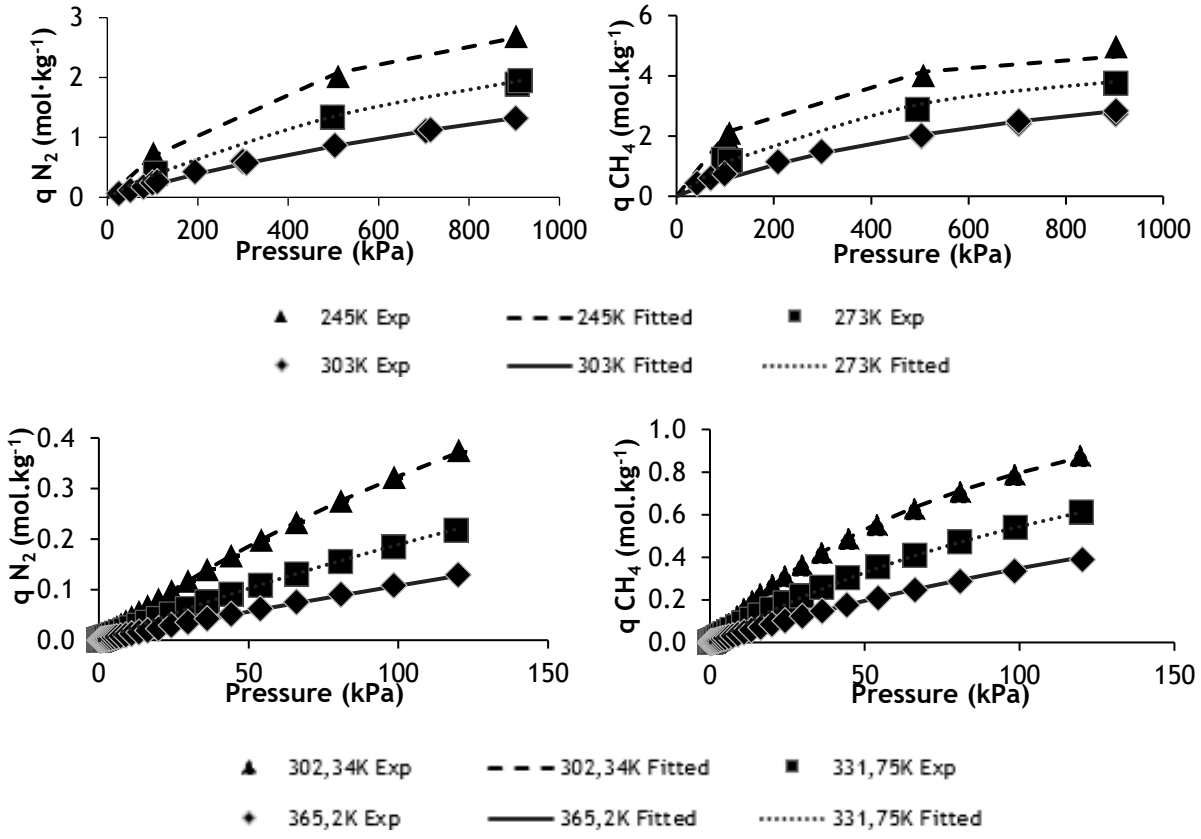


*Figure 6. Experimental and correlated isotherms for pure $N_2$ (left) and pure $CH_4$ (right) on Norit RB-3 (upper) and CMS-3K 172 (lower).*

The estimated Langmuir isotherm parameters (in the unit format specified within the software package) as well as the RMSE of the regression are presented in Table 3. Additionally, the mass transfer coefficients obtained for each adsorbent are also represented.

*Table 3. Estimated Langmuir isotherm parameters and respective statistical uncertainties.*

| | | $Q \times 10^{-3}$ (kmol.kg$^{-1}$) | $b_0 \times 10^{-4}$ (bar$^{-1}$) | $(-\Delta H) \times 10^{7}$ (J.kmol$^{-1}$) | RMSE (kmol.kg$^{-1}$) | $k_{LDF}$ (s$^{-1}$) |
|---|---|---|---|---|---|---|
| **Norit-RB 3** | $CH_4$ | 5.50 | 1.19 | 1.74 | $1.10 \times 10^{-4}$ | 1 |
| | $N_2$ | 4.19 | 1.85 | 1.42 | $3.72 \times 10^{-5}$ | 3 |
| **CMS-3K 172** | $CH_4$ | 1.60 | 6.05 | 1.86 | $3.53 \times 10^{-6}$ | $1.26\times 10^{-4}$ |
| | $N_2$ | 1.30 | 1.73 | 1.90 | $7.85 \times 10^{-7}$ | 0.015 |

Relatively to the carbon molecular sieve, if only the equilibrium capacities were considered it would be equilibrium selective for $CH_4$. However, the mass transfer coefficient difference proves that it is in fact, kinetically selective for $N_2$. In Table 4, the Extended Langmuir isotherm parameters (IP) are represented in the format that the software demands.

*Table 4. Extended Langmuir 2 isotherm parameters (IP).*

| | | $IP_1 \times 10^{-7}$ (kmol.bar$^{-1}$.kg$^{-1}$) | $IP_2$ (K) | $IP_3 \times 10^{-4}$ (bar$^{-1}$) | $IP_4$ (K) |
|---|---|---|---|---|---|
| **Norit-RB 3** | $CH_4$ | 6.55 | 2087 | 1.19 | 2087 |
| | $N_2$ | 7.74 | 1704 | 1.84 | 1704 |
| **CMS-3K 172** | $CH_4$ | 9.68 | 2237 | 6.05 | 2237 |
| | $N_2$ | 2.25 | 2285 | 1.73 | 2285 |

These regressed parameters differ only slightly from those obtained by Zhang et al. (2016) [46] for the Norit RB-3 and by Xiao et al. (2019) [21] for the carbon molecular sieve.

## 4.2 Adsorption bed parameters

Here, the specific adsorption bed parameters required from the material and energy balance previously described, which will be used for this work are listed in Table 5.

*Table 5. Column parameters and constants used throughout the simulations.*

| Parameter | Norit-RB 3 | CMS-3K 172 |
|---|---|---|
| **Number of nodes, $N$** | 10 | |
| **$D_L$ (m$^2$.s$^{-1}$)** | $3.8\times 10^{-5}$ | |
| **Wall thickness (m)** | 0.0015 | 0.0016 |

| | |
|---|---|
| $C_{pw}$ (J.kg$^{-1}$.K$^{-1}$) | 500 |
| $k_w$ (MW.m$^{-1}$.K$^{-1}$) | $1.600\times 10^{-5}$ |
| $\rho_w$ (kg.m$^{-3}$) | 7800 |
| $H_{amb}$ (MW.m$^{-2}$.k$^{-1}$) | 0.003 |
| $H_w$ (MW.m$^{-2}$.k$^{-1}$) | 0.003 |

Furthermore, parameters such as the column length, diameter, interstitial velocity, among others will be optimized in the following chapters. The operating parameters that were used as a baseline for all the upcoming simulations are displayed in Table 6.

*Table 6. Operating parameters used as a starting point for all the simulations.*

| Operating Parameter | |
|---|---|
| $F$ (Nm$^3$.h$^{-1}$) | 500 |
| Feed Pressure, $P_F$ (bar) | 11 |
| Low Pressure, $P_L$ (bar) | 1.013 |
| $T_{amb}$ (K) | 298.15 |
| $T_g$ (K) | 298.15 |

## 4.3 Dynamic analysis with breakthrough curves

To properly predict the behaviour of the adsorbent and to confirm the adsorption equilibrium curves and the kinetic data under the given operating conditions, pure gas and binary breakthrough curves were simulated. Thus, a simple apparatus was assembled as seen in Figure 7 where VF (feed valve) is open with a constant flowrate, VP (product valve) is completely open and the adsorption bed is initially filled with 100% of $N_2$.

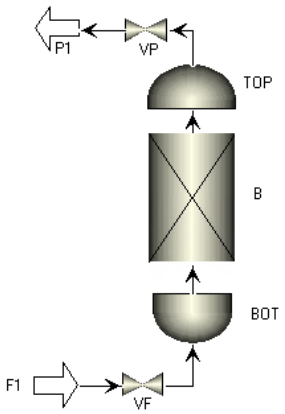


*Figure 7. Process flowsheet for the breakthrough study.*

### 4.3.1 Norit-RB 3

Based on the strategy delineated in Chapter 3.5 an initial estimation of the size of the adsorbing column was done for a flowrate of 500 $Nm^3.h^{-1}$. By assuming a ratio of $U_i/U_{mf}$ equal to 0.3 and a ratio of 5 for L/D to approximate a plug flow behavior, an adsorbent column with a diameter of 0.27 m, a length of 1.37 m and a superficial velocity of 0.23 $m.s^{-1}$ was designed. The adsorption of the binary mixture of $CH_4/N_2$ (80/20 %) in the industrial-scale bed was simulated with these features and the obtained results are represented in Figure 8, while the results for the breakthrough curve obtained for pure $CH_4$ are in Appendix I.

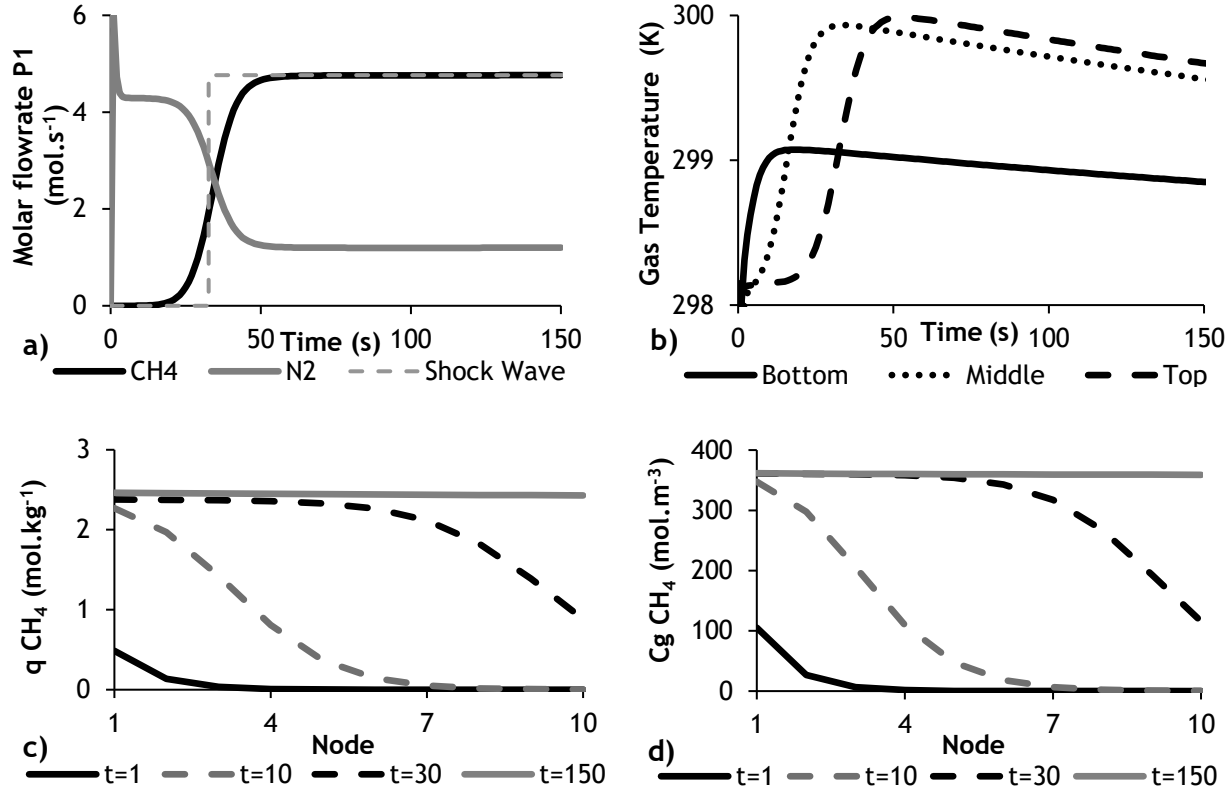


*Figure 8. Simulation results for the binary breakthrough curve for F=500 $Nm^3.h^{-1}$, D=0.27 m, L=1.37 m, $U_s$=0.23 $m.s^{-1}$ where a) molar flowrate history at P1; b) gas temperature along the column for N=1, N=5 and N=10; evolution of the solid phase (c) and gas phase concentration profiles.*

In Figure 8a), the breakthrough curve shows reasonable dispersion due to the contribution of the axial dispersion and mass transfer coefficients. Additionally, considering no contribution from such resistances, the shock wave was predicted based on the equality of the area below the curve for $CH_4$ before the stoichiometric time and the area of the curve given by the difference between the steady state molar flowrate of $CH_4$ and the $CH_4$ curve after the $t_{st}$, a method based on the conservation of mass. For the predicted shock wave the $t_{st}$ was given at 33 s while the theoretical one, calculated with Equation (16), was given at 19 s. Also the breakthrough point happened at 23 s, which implies that the adsorption time should be smaller

or equal to 23 s. The LUB was calculated as -0.29 m which corresponds to a new column length of 1.08 m. Relatively to Figure 8c), the adsorbed amount of $CH_4$ at equilibrium corresponds to 2,44 $mol_{CH4}.kg^{-1}_{ads}$ which is coherent with the calculated one from the pure component equilibrium isotherm for $CH_4$ at the partial pressure of 8.8 bar and temperature of 298.15 K: 2.95 $mol_{CH4}.kg^{-1}_{ads}$. Any difference between the two is due to the fact that one value was calculated considering pure components only while the other already takes into account the multi-component adsorption phenomenon.

No further work was pursued with this adsorbent after simulations tests done for a 4-step PSA and a 6-step PSA with Pressure Equalization step revealed that even though at the top product there was a significant increase in $N_2$ composition and a decrease in $CH_4$, at the Waste outlet no enrichment of the heavier component was verified.

### 4.3.2 CMS-3K 172

Similarly to the assumptions made for the activated carbon, a ratio of $U_i/U_{mf}$ equal to 0.3 and a ratio of 3 for L/D, a first estimation of the bed sizing for the CMS was done with D= 0.80 m, L=2.41 m and $U_s$=0.03 $m.s^{-1}$. The breakthrough curve for the binary mixture of $CH_4/N_2$ (80/20 %) was simulated and the results are represented in Figure 9 while the evolution of both gas phase and solid phase for both components are represented in Appendix J.

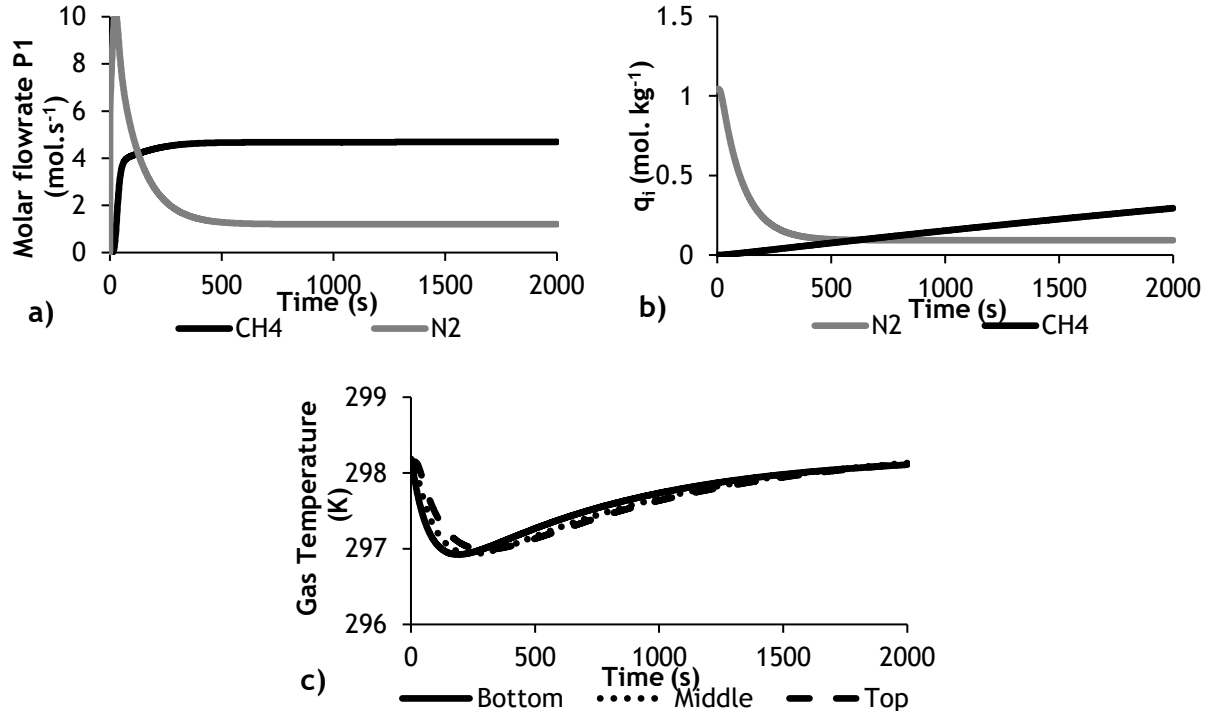


*Figure 9. Simulation results for the binary breakthrough curve for a flowrate of 500 $Nm^3.h^{-1}$, D=0.80 m, L=2.41 m, $v_s$=0.03 $m.s^{-1}$ where a) molar flowrate history at P1; b) amount adsorbed evolution of particles at the end of the column; c) gas phase temperature along the column for N=1, N=5 and N=10.*

By comparing Figure 9 a) and b) we can conclude that even when the molar flowrate at the product stream appears to get to a steady state, the adsorbent is still adsorbing methane, and will be until it reaches the adsorption equilibrium at 1.45 $mol_{CH4}.kg^{-1}_{ads}$. Regarding Figure 9 c), the temperature decrease is due to the fact that initially the bed is filled with $N_2$, hence residual desorption occurs at the beginning of the simulation, lowering the temperature. Afterwards, the temperature stabilizes at 298 K confirming the isothermal behavior of this system, even though slight temperature increments are expected due to the released heat of adsorption during this step. Even though the difference in the kinetics of $N_2$ and $CH_4$ is incredibly large, the amount of methane that is adsorbed is considerable.

Expectedly, the obtained results for this kinetic adsorbent differ from the ones achieved for the CMS since instead of a shock wave where the breakthrough happens almost instantly, the kinetic effects due to mass diffusional limitations, extend the breakthrough in time.

In order to understand the dynamic behavior of this separation, breakthrough curves for different flowrates but the same column dimensions are represented in Figure 10 as well as a study of the different kinetics for each example in Table 7.

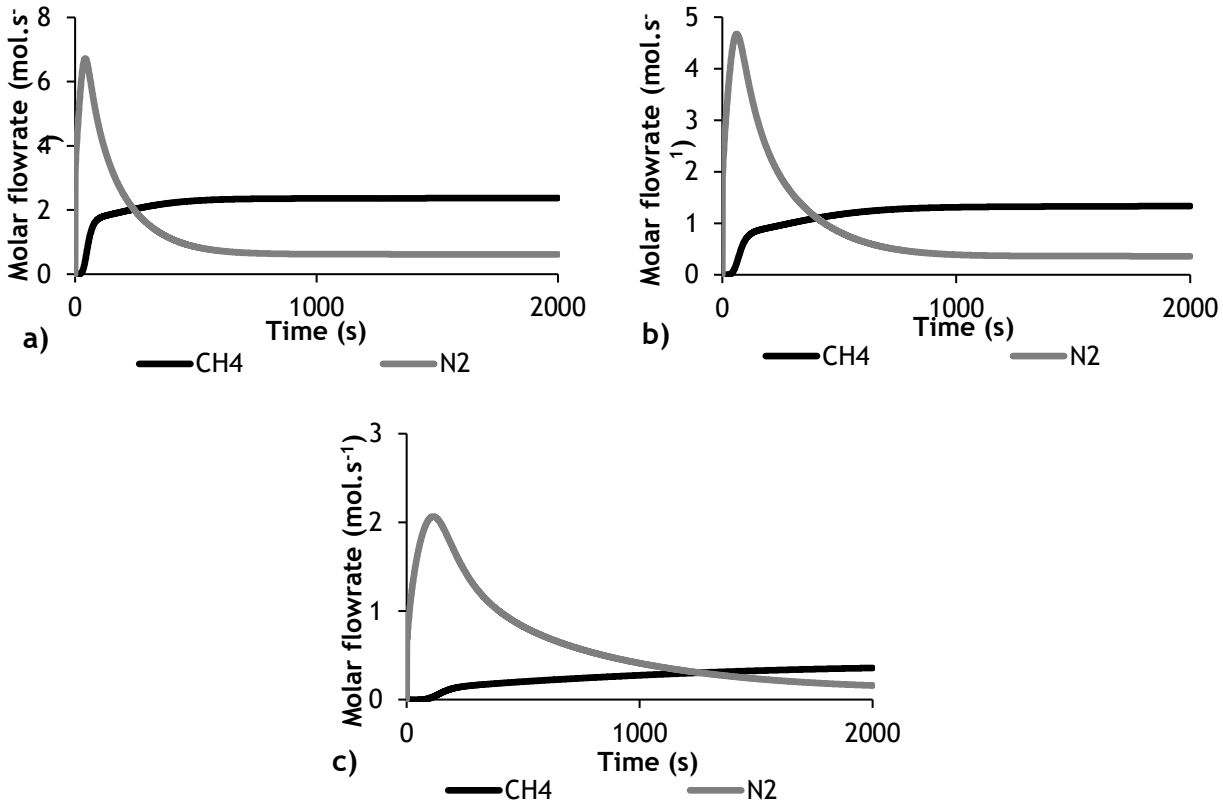


*Figure 10. Binary breakthrough curves for D=0.80 m and L=2.41 m and different flowrates a)250 $Nm^3.h^{-1}$ b)150 $Nm^3.h^{-1}$c)50 $Nm^3.h^{-1}$.*

*Table 7. Kinetic analysis for the different flowrates.*

| $F$ (Nm$^3$.h$^{-1}$) | $F$ (kmol.s$^{-1}$) | $U_s$ (m.s$^{-1}$) | $U_i$ (m.s$^{-1}$) | $\tau$ (s) | $t_{diff_{CH_4}}$ (s) | $t_{diff_{N_2}}$ (s) |
|---|---|---|---|---|---|---|
| **500** | 0.0061 | 0.0030 | 0.0092 | 87 | $7.9 \times 10^3$ | 67 |
| **250** | 0.0031 | 0.0015 | 0.0046 | 175 | $7.9 \times 10^3$ | 67 |
| **150** | 0.0018 | 0.00091 | 0.0027 | 291 | $7.9 \times 10^3$ | 67 |
| **50** | 0.00061 | 0.00030 | 0.00092 | 873 | $7.9 \times 10^3$ | 67 |

For the separation to be driven by mass transfer the variable $\tau$ should be slightly higher than 67 s ($t_{diff_{N_2}}$) but much lower than 7900 s ($t_{diff_{CH_4}}$) to prevent the adsorption of methane. Hence, for this column's parameters all of these different flowrates seem to be adequate to effectively perform this separation controlled by the kinetics.

## 4.4 PSA simulations with CMS-3K 172

Belatedly, an error was found in the simulations that will follow. Incorrect equilibrium data was given as an input to the software Aspen Adsorption which is behind some incoherencies in the gas phase graphics which will be shown, especially for methane. Nonetheless, this error is not expected to have a meaningful impact in the system since the separation is driven by the kinetics and not by the equilibrium.

### 4.4.1 4-Step Cycle parametric study

The study started with a 2-column with D=0.80 m and L=2.41 m, 4-step cycle (equal to the one in Figure 4) comprising feed pressurization (PR), high-pressure adsorption (AD), counter-current blowdown (BL) and a purge (PU) where PR/PU and AD/BL always work in pairs between the 2 columns. The process flowsheet for this simulation is represented in Figure 11 and as initial conditions the columns were filled with nitrogen at the feed temperature while relatively to the pressure both columns were at the zero time pressure that preceded each first step. Hence, while the B1 started at 1.013 bar, B2 started at the feed pressure (11 bar). Furthermore, the specification of each valve represented in Figure 11 is laid out in Table 8. VF, VP, VW and VPU were all implemented as control valves with their flow rate set according to the pressure that goes across (2) them while the rest are either open (1) or closed (0).

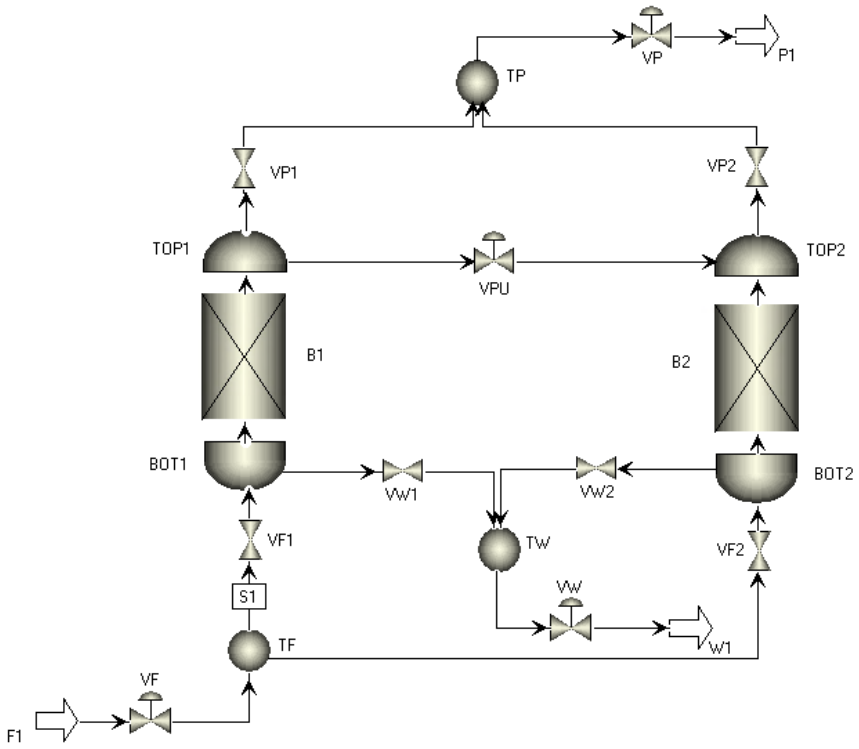


*Figure 11. Process flowsheet of the 4-step and 6-step cycles simulations*

*Table 8. Valves' specifications (.spec) and valve CV coefficient (.CV) if it is applicable for the 4-step PSA simulation.*

| | PR/BL | AD/PU | BL/PR | PU/AD |
|---|---|---|---|---|
| **VF.spec** | 2 | 2 | 2 | 2 |
| **VF.CV (kmol.s$^{-1}$.bar$^{-1}$)** | $6 \times 10^{-4}$ | | | |
| **VF1.spec** | 1 | 1 | 0 | 0 |
| **VF2.spec** | 0 | 0 | 1 | 1 |
| **VPU.spec** | 0 | 2 | 0 | 2 |
| **VPU.CV (kmol.s$^{-1}$.bar$^{-1}$)** | $6 \times 10^{-5}$ | | | |
| **VP.spec** | 2 | 2 | 2 | 2 |
| **VP.CV (kmol.s$^{-1}$.bar$^{-1}$)** | $3.1 \times 10^{-4}$ | | | |
| **VP1.spec** | 0 | 1 | 0 | 0 |
| **VP2.spec** | 0 | 0 | 0 | 1 |
| **VW.spec** | 2 | 2 | 2 | 2 |
| **VW.CV (kmol.s$^{-1}$.bar$^{-1}$)** | $6.3 \times 10^{-4}$ | | | |

| | | | | |
|---|---|---|---|---|
| **VW1.spec** | 0 | 0 | 1 | 1 |
| **VW2.spec** | 1 | 1 | 0 | 0 |
| **t (s)** | 180 | 80 | 180 | 80 |

The performance of the PSA system for this cycle configuration, evaluated by the three parameters previously described, was given by: 97% $CH_4$ purity; 39% $CH_4$ recovery; 4.1 $mol_{CH_4}.kg_{ads}^{-1}.h^{-1}$ productivity. In Figure 12 a) the evolution of the CH4 purity and recovery throughout the number of cycles is given and it infers that the cyclic steady state (CSS) is achieved after 217 cycles which corresponds to 1 day and 7h. This is owed, mainly, to the time that it takes for the temperature profile within the bed to stabilize.

Regarding the gas temperature along the bed at CSS, in Figure 12 c), the obtained profile demonstrates the isothermal characteristic of this system, with slight increases in temperature during adsorption and decreases in the purge step.

Considering the pressure of the two beds at steady state, in Figure 12 b), it is noticeable that the adsorption step does not occur at constant pressure which is a direct consequence of using a CV coefficient in the product valve (VP) so close to that of the feed valve (VF). Also, the pressure range within both beds does not comprehend the totality predicted for this study which may be caused by the low PR/BL step time and correlated with the CV.VP. Nonetheless, the driven force in the column to pressurize or depressurize at the beginning of these steps is high enough so that the process occurs normally without constraints. Along each step, the driven force diminishes which may comprehend the fact that an increase of the PR/Bl time may never solve this problem.

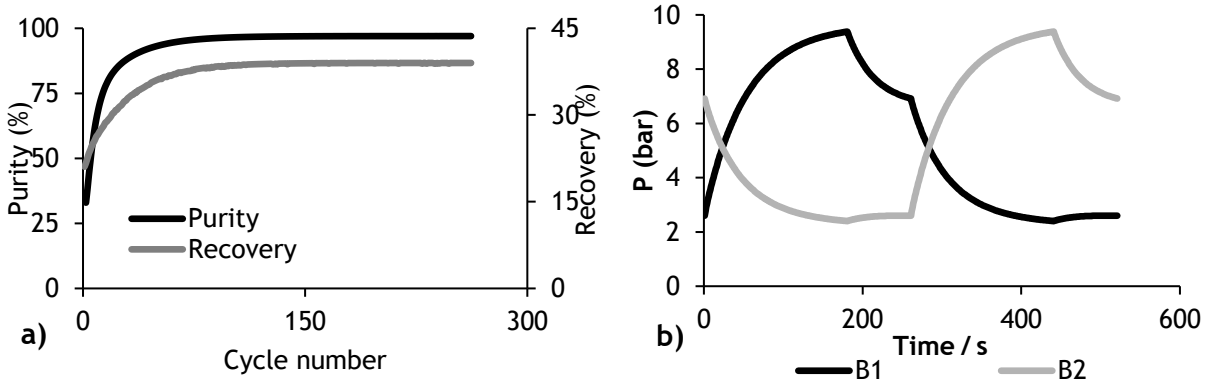

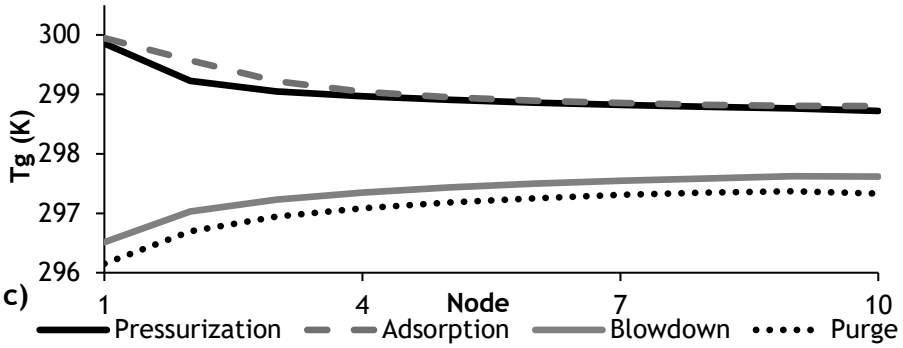


*Figure 12. Simulation results for the 4-step PSA for F=500 Nm$^3$.h$^{-1}$, L/D=3, $U_i/U_{mf}$=0.3 where: a) evolution of the $CH_4$ purity and recovery with the cycle number; b) pressure obtained at the column outlet at CSS; c) Gas temperature profile along the bed at the end of each step at CSS.*

Furthermore, on the simulation results, the gas phase and solid phase profiles for both components along the bed at CSS are given in Figure 13.

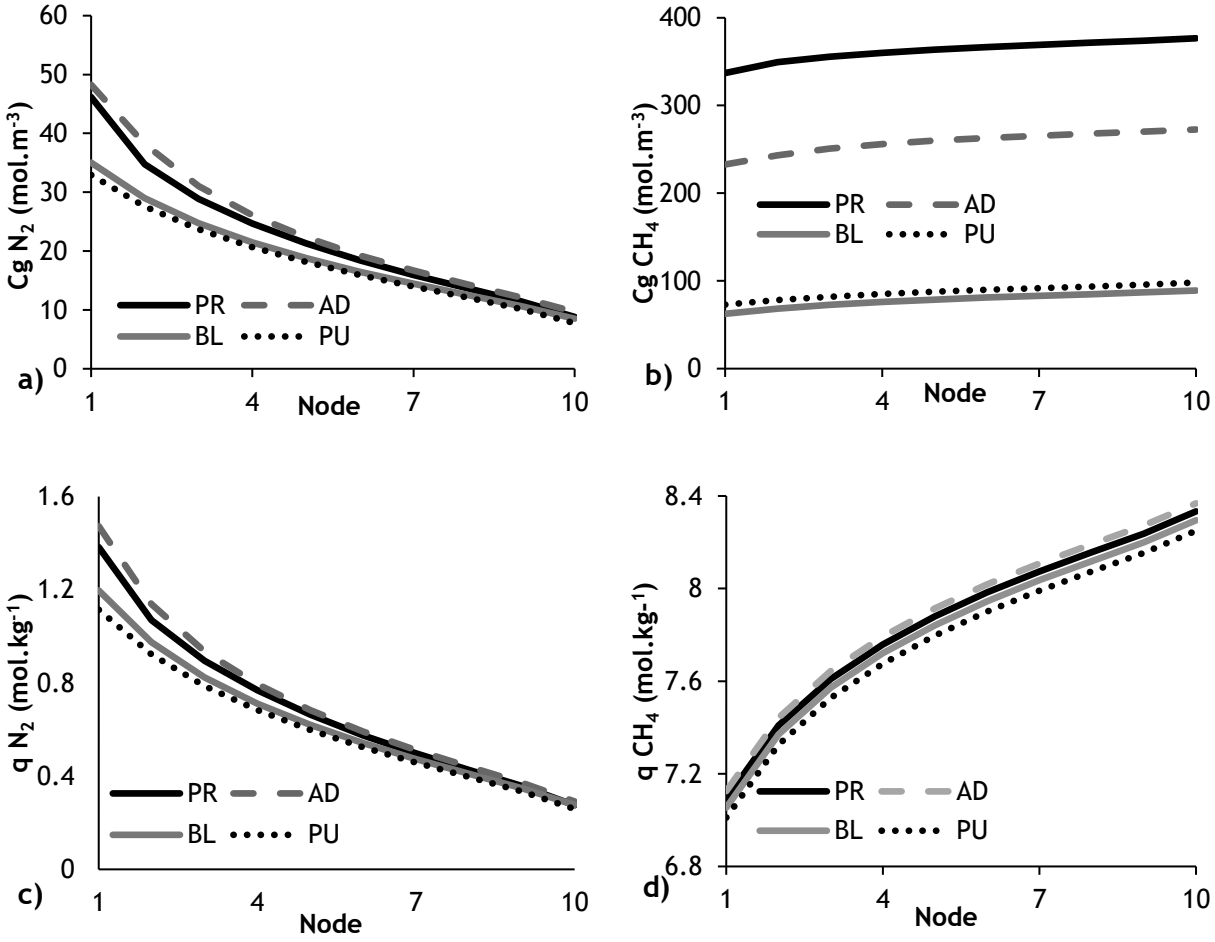

*Figure 13. Gas phase (a and b) and solid phase (c and d) concentration profiles for $N_2$ (a and c) and $CH_4$ (b and d) at CSS obtained for the 4-step PSA for F=500 $Nm^3.h^{-1}$, L/D=3, $U_i/U_{mf}$=0.3.*

Analysing the graphics for methane, which has slow kinetics, even though its concentration in the fluid phase (Figure 13b)) between steps varies a lot, the solid phase does not (Figure 13d)). So, the adsorbed amount of methane is kept constant for each step after reaching a certain equilibrium.

Regarding Figure 13c), for nitrogen, the working capacity of the bed between the feed step and the regeneration is small but there is room for improvement if this cycle is optimized.

In order to get an insight of how certain parameters such as the CV coefficient of VP (VP.CV), the AD/PU and PU/AD step time ($t_{ads}$), the feed pressure ($P_F$), the ratio $U_i/U_{mf}$, the ratio L/D and the heavy flow to feed ratio (H/F) can influence the system performance a parametric study is represented in Figure 14. The methane purity decreases with the increase of the VP.CV (graphic a)), the AD/PU and PU/AD time (graphic b)) and the ratio L/D (graphic e)). For the first two parameters, the recovery is increased with the purity decrease whereas for the ratio L/D the recovery also decreases. On the other hand, the methane purity increases with the increase of the $P_F$ (graphic c)) and the ratio H/F (graphic f)). A slight increase in the recovery is verified with the increase of $P_F$ whilst a decrease of this variable is verified with the increase of the ratio H/F. A different trend is observed for the ratio $U_i/U_{mf}$ (graphic d)) where the $CH_4$ purity increases until a maximum it attained for a ratio of 0.4 and a purity of 97.35 after which this variable starts to decrease. Relatively to the recovery, it increases along with this ratio. In this case, the inversion point occurs when the adsorbent length in no longer sufficient to retain the nitrogen.

The plot f) demonstrates the influence of these parameters on the process purity and recovery. When analyzing the ratio H/F, even though it has a considerable influence on the process purity it shows very little effect on the recovery. The $P_F$ shows a generally low influence, having a very small impact on the product recovery and an average one on the purity. Alternatively, the influence of the ratio $U_i/U_{mf}$ and the VP.CV is considerable on the overall process performance. Even so, the interaction between these two parameters is interesting since for the same recovery, higher purities are exhibited for the change in the VP.CV but only until an inversion point for recoveries higher than 45% where the opposite is verified. Regarding the influence of the $t_{ads}$ and the ratio L/D it is minor when compared to the impact of other parameters, although they do show a considerable influence on the process recovery.

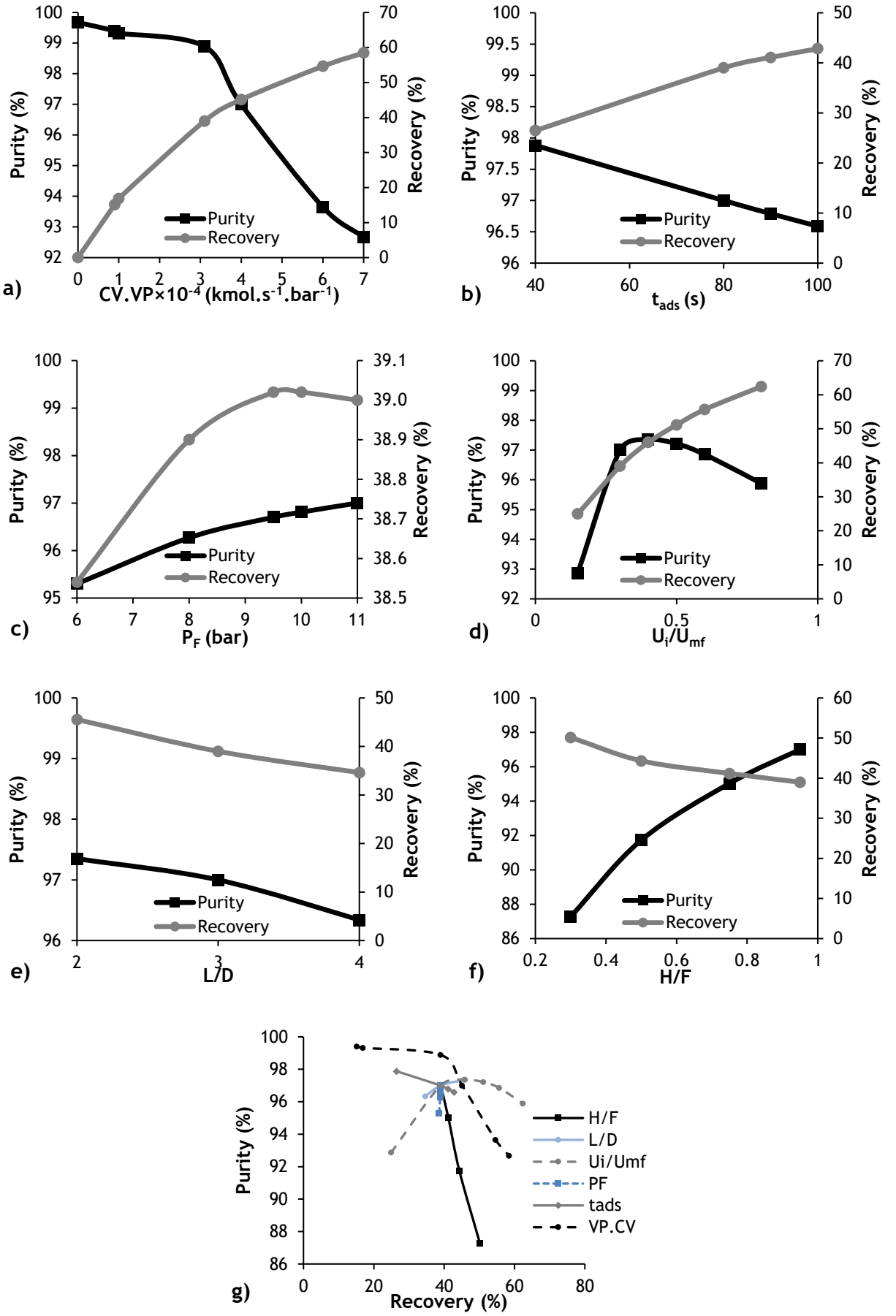
a)
Purity (%)
Recovery (%)
CV.VP×10-4 (kmol.s-1.bar-1)
Purity
Recovery
b)
tads (s)
c)
PF (bar)
d)
Ui/Umf
e)
L/D
f)
H/F
g)
H/F
L/D
Ui/Umf
PF
tads
VP.CV
Recovery (%)

*Figure 14. Parametric study at CSS according to the purity and recovery of $CH_4$ for the 4-step PSA for F=500 $Nm^3.h^{-1}$ where the CV.VP a), the $t_{ads}$ b), the $P_F$ c), the ratio $U_i/U_{mf}$ d), the ratio L/D e) and the ratio H/F f) operating parameters were studied and the comparison of the studied parameters effect on the system performance g).*

### 4.4.2 6-step cycle optimization

At this stage, two steps were added to the 4-step cycle, namely, two pressure equalizations (PEq), an implementation aimed to enhance the $CH_4$ recovery as previously explained in Chapter 2.4.3.2. The PSA apparatus is represented in the former Figure 11 and the column's steps arrangement is represented in Figure 15. Initially, both columns were filled with nitrogen and at the feed temperature although the initial pressure for each column was the one related to that of the zero time of the first step, so, both columns started at 6 bar.

| | | | | | | |
|---|---|---|---|---|---|---|
| B1 | PR | AD | PEq | BL | PU | PEq |
| B2 | BL | PU | PEq | PR | AD | PEq |

*Figure 15. 2-column arrangement for the 6-step PSA.*

Moreover, an optimization based on the parametric study for the 6-step PSA was carried out where the CV coefficient of VP (VP.CV), the AD/PU and PU/AD step time ($t_{ads}$), the feed pressure ($P_F$), the ratio $U_i/U_{mf}$, the ratio L/D, the heavy flow to feed ratio (H/F), the PR/BL and BL/PR step time ($t_{press}$), the CV used in the purge valve during the pressure equalization steps (CV.VPU.PEq) and the pressure equalization time ($t_{PEq}$) were varied as demonstrated in Table 9. The criteria used to choose the 6-step PSA configuration was based on fixing the $CH_4$ purity at 97% to obtain the highest possible $CH_4$ recovery for the minimum required purity. The results for each simulation are presented in Table 10.

*Table 9. 6-step PSA optimization parameters for 11 different simulations.*

| Run | $t_{ads}$ (s) | CV.VP $\times 10^{-4}$ ($kmol.s^{-1}.bar^{-1}$) | H/F | $t_{press}$ (s) | L/D | $U_i/U_{mf}$ | $P_F$ (bar) | CV.VPU.PEq $\times 10^{-4}$ ($kmol.s^{-1}.bar^{-1}$) | $t_{PEq}$ (s) |
|---|---|---|---|---|---|---|---|---|---|
| **(1)** | 80 | 3.1 | 0.95 | 180 | 3 | 0.3 | 11 | 0.6 | 180 |
| **(2)** | 100 | 2 | 0.75 | 230 | 2 | 0.8 | 11 | 1 | 60 |
| **(3)** | 100 | 1 | 0.50 | 170 | 2 | 0.8 | 11 | 1 | 70 |
| **(4)** | 100 | 3.1 | 0.50 | 170 | 2 | 0.8 | 11 | 3 | 70 |
| **(5)** | 100 | 3.1 | 0.85 | 170 | 2 | 0.8 | 11 | 1 | 70 |
| **(6)** | 100 | 2 | 0.75 | 170 | 2 | 0.8 | 11 | 1 | 70 |

| | | | | | | | | | |
|---|---|---|---|---|---|---|---|---|---|
| **(7)** | 100 | 3.1 | 0.95 | 170 | 2 | 0.8 | 11 | 1 | 70 |
| **(8)** | 100 | 2 | 0.85 | 230 | 2 | 0.8 | 11 | 1 | 70 |
| **(9)** | 100 | 1.7 | 0.95 | 230 | 2 | 0.8 | 11 | 1 | 60 |
| **(10)** | 100 | 2 | 0.95 | 220 | 2 | 0.8 | 11 | 1 | 80 |
| **(11)** | 100 | 1.5 | 0.85 | 200 | 2 | 0.8 | 11 | 1 | 70 |

*Table 10. 6-step PSA optimization results for 11 different simulations.*

| Run | Purity (%) | Recovery (%) | Productivity ($mol_{CH_4}.kg_{ads}^{-1}.h^{-1}$) |
|---|---|---|---|
| **(1)** | 98.52 | 43.23 | 2.43 |
| **(2)** | 96.66 | 63.66 | 14.7 |
| **(3)** | 98.49 | 50.99 | 9.79 |
| **(4)** | 91.73 | 75.45 | 22.4 |
| **(5)** | 93.55 | 74.04 | 22.5 |
| **(6)** | 96.08 | 66 | 16.8 |
| **(7)** | 94.14 | 75.6 | 22.1 |
| **(8)** | 97.02 | 63.25 | 14.4 |
| **(9)** | 98.08 | 58.97 | 12.7 |
| **(10)** | 97.15 | 63.36 | 14.3 |
| **(11)** | 98.11 | 53.74 | 12.5 |

According to the previously mentioned criterium, the set of operating parameters which exhibited the optimized process performance was those used in run (10) for a height of 1 m and a diameter of 0.5 m. The simulation results for this run are displayed in Figure 16 and Figure 17. The history of pressures during a cycle (Figure 16b)) at CSS, reached after 91 cycles, shows that for this improved 6-step cycle the adsorption and purge steps occur at constant pressure. Regarding the evolution of the gas temperature during a cycle, as expected, the temperature increases during the adsorption step.

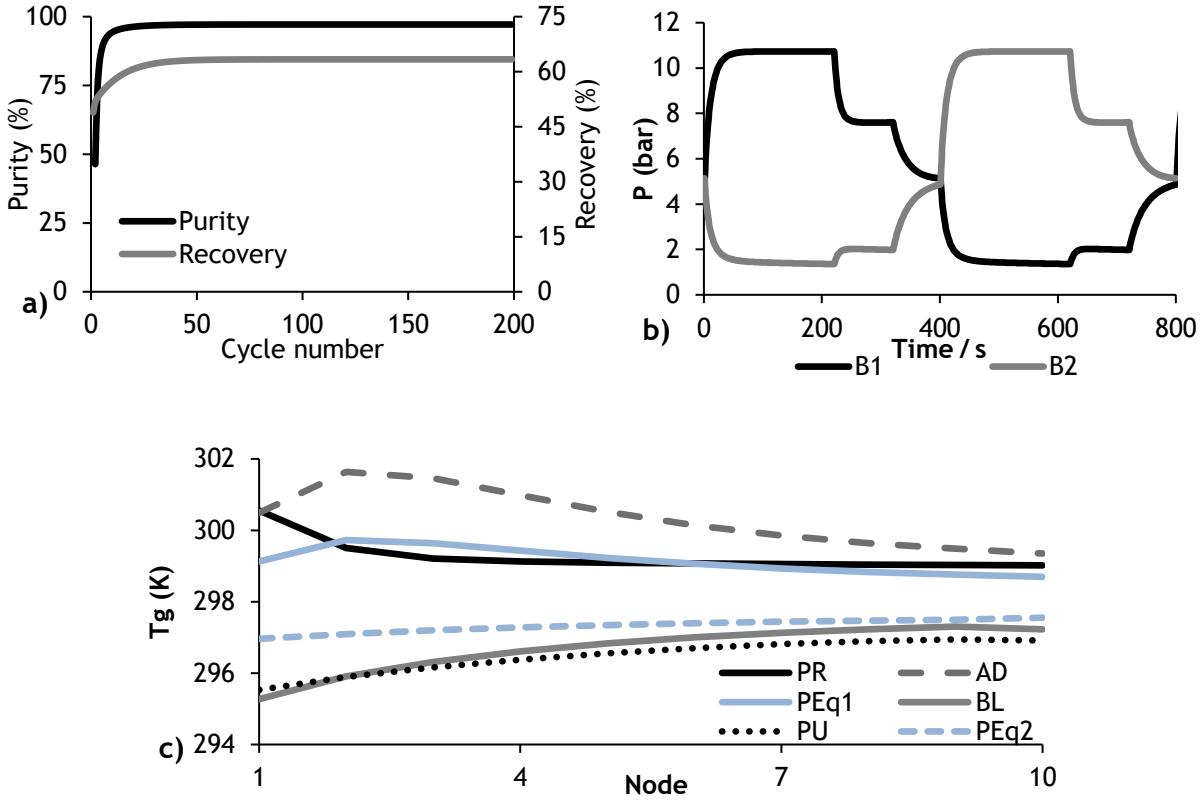


*Figure 16. Simulation results for the 6-step PSA for F=500 $Nm^3.h^{-1}$, L/D=2, $U_i/U_{mf}$=0.8 where: a) evolution of the $CH_4$ purity and recovery with the cycle number; b) pressure obtained at the column outlet at CSS; c) Gas temperature profile along the bed at the end of each step at CSS.*

To further evaluate this simulation, the gas phase and solid phase profiles for both components along the bed at CSS are given in Figure 17. As expected, the difference between the uptake at the feed and purge step is higher for nitrogen when comparing with the 4-step cycle which is related with the higher performance delivered for this optimized cycle.

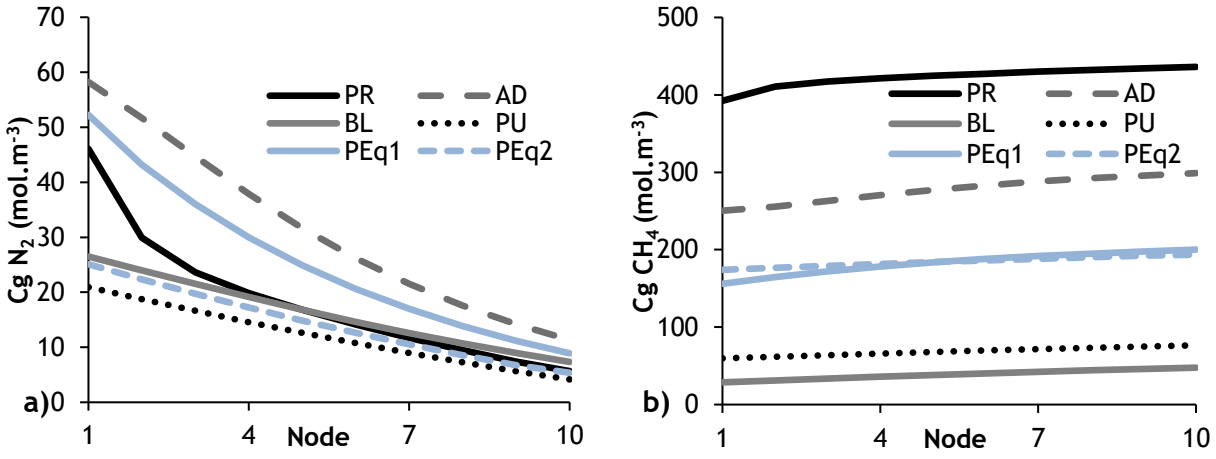

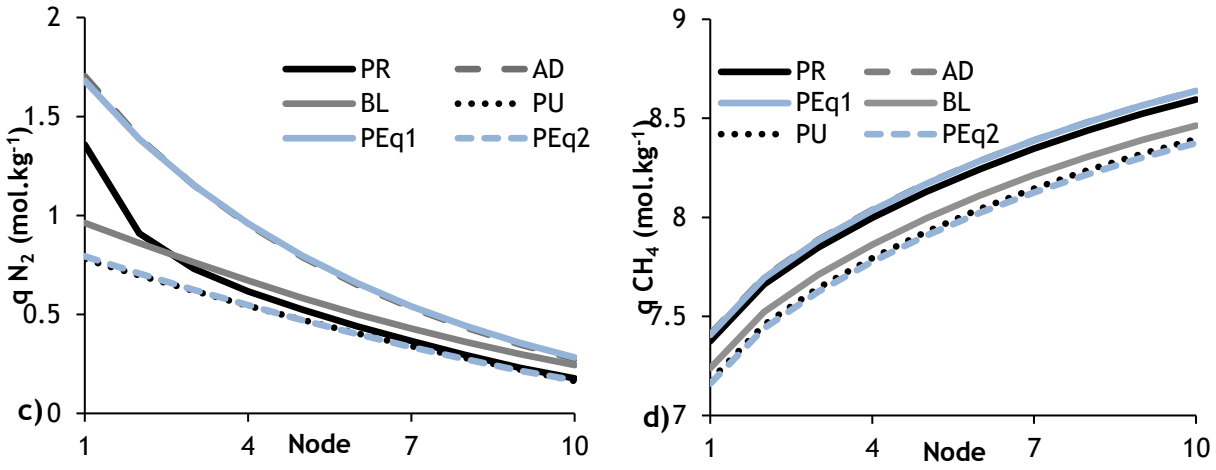


*Figure 17. Gas phase (a and b) and solid phase (c and d) concentration profiles for $N_2$ (a and c) and $CH_4$ (b and d) at CSS obtained for the 6-step PSA for F=500 $Nm^3.h^{-1}$, L/D=2, $U_i/U_{mf}$=0.8.*

Additionally, a feed composition test for the optimized operating parameters was produced to look at how different compositions of the inlet stream such as 90/10% and 85/15% and 75/25 of $CH_4/N_2$, affects the system performance. The results obtained are represented in Table 11.

*Table 11. Simulation results for the 6-step PSA for F=500 $Nm^3.h^{-1}$, L/D=2, $U_i/U_{mf}$=0.8 while varying the feed composition.*

| $CH_4/N_2$ (%) | Purity (%) | Recovery (%) | Productivity ($mol_{CH_4}.kg_{ads}^{-1}.h^{-1}$) |
|---|---|---|---|
| **80/20** | 97.15 | 63.36 | 14.3 |
| **90/10** | 98.72 | 62.97 | 14.9 |
| **85/15** | 97.98 | 63.17 | 14.7 |
| **75/25** | 96.80 | 63.51 | 14.5 |

Hence, if the feed composition changes it is expected not to have a meaningful impact on the process performance.

### 4.4.3 An improved PSA cycle: 8-step cycle

To further improve the 6-step cycle PSA, a new 8-step cycle was designed, schematically shown in Figure 18. The added step occurs after the adsorption as a co-current blowdown (BLCo) to maximize the harvest of the gas within the inter-particle pores.

*Figure 18. 2-column working schedule for the 8-step cycle PSA.*

| | | | | | | | | |
|---|---|---|---|---|---|---|---|---|
| B1 | PR | AD | BLCo | PEq | BL | PU | | PEq |
| B2 | BL | PU | | PEq | PR | AD | BLCo | PEq |

In order to optimize this 8-step cycle a study was conducted where operating parameters were varied such as the $t_{BLCo}$, the CV.VP, the CV used in the purge valve during the BLCo steps (CV.VPU.BLCo), the $t_{ads}$, the $t_{press}$ and the $t_{PEq}$. The rest of the parameters were the same as those used in run (11) for the 6-step PSA. 8 different runs were performed and the parameters were varied as shown in Table 12. The process performance for each run is displayed in Table 13 where the optimized cycle configurations were decided based on the same criteria used in the 6-step process optimization.

*Table 12. 8-step PSA optimization parameters for 8 different simulations.*

| Run | CV.VP $\times 10^{-4}$ ($kmol.s^{-1}.bar^{-1}$) | CV.VPU.BLCo $\times 10^{-4}$ ($kmol.s^{-1}.bar^{-1}$) | $t_{press}$ (s) | $t_{ads}$ (s) | $T_{BLCo}$ (s) | $t_{peq}$ (s) |
|---|---|---|---|---|---|---|
| **(1)** | 2 | 0.6 | 220 | 100 | 25 | 80 |
| **(2)** | 2 | 0.6 | 230 | 150 | 35 | 50 |
| **(3)** | 2 | 0.01 | 230 | 180 | 50 | 50 |
| **(4)** | 1.5 | 0.01 | 230 | 120 | 50 | 40 |
| **(5)** | 1.5 | 0.01 | 230 | 160 | 50 | 50 |
| **(6)** | 1.5 | 0.01 | 230 | 160 | 50 | 40 |
| **(7)** | 1.4 | 0.01 | 230 | 100 | 75 | 50 |
| **(8)** | 1.5 | 0.01 | 230 | 130 | 75 | 50 |

*Table 13. 8-step PSA optimization results for 8 different simulations.*

| Run | Purity (%) | Recovery (%) | Productivity ($mol_{CH_4}.kg_{ads}^{-1}.h^{-1}$) |
|---|---|---|---|
| **(1)** | 96.49 | 67.50 | 15.2 |
| **(2)** | 95.44 | 70.74 | 20.2 |
| **(3)** | 94.79 | 72.16 | 21.9 |
| **(4)** | 97.21 | 65.00 | 14.9 |
| **(5)** | 96.44 | 67.67 | 17.8 |
| **(6)** | 96.78 | 66.22 | 17.4 |
| **(7)** | 97.44 | 64.40 | 12.4 |

| | | | |
|---|---|---|---|
| **(8)** | 96.97 | 66.05 | 14.5 |

According to the previously mentioned criterium, the set of operating parameters which exhibited the optimized process performance were those used in run (8) and its simulation results are displayed in Figure 19 and Figure 20. Nonetheless, since for the run (4), the productivity was higher, this cycle configuration was also considered and its results are represented in Appendix K. In Figure 19 it is shown that the cycle gets to CSS at cycle number 66 and the pressure evolution graphic is as expected due to the used valve's CV.

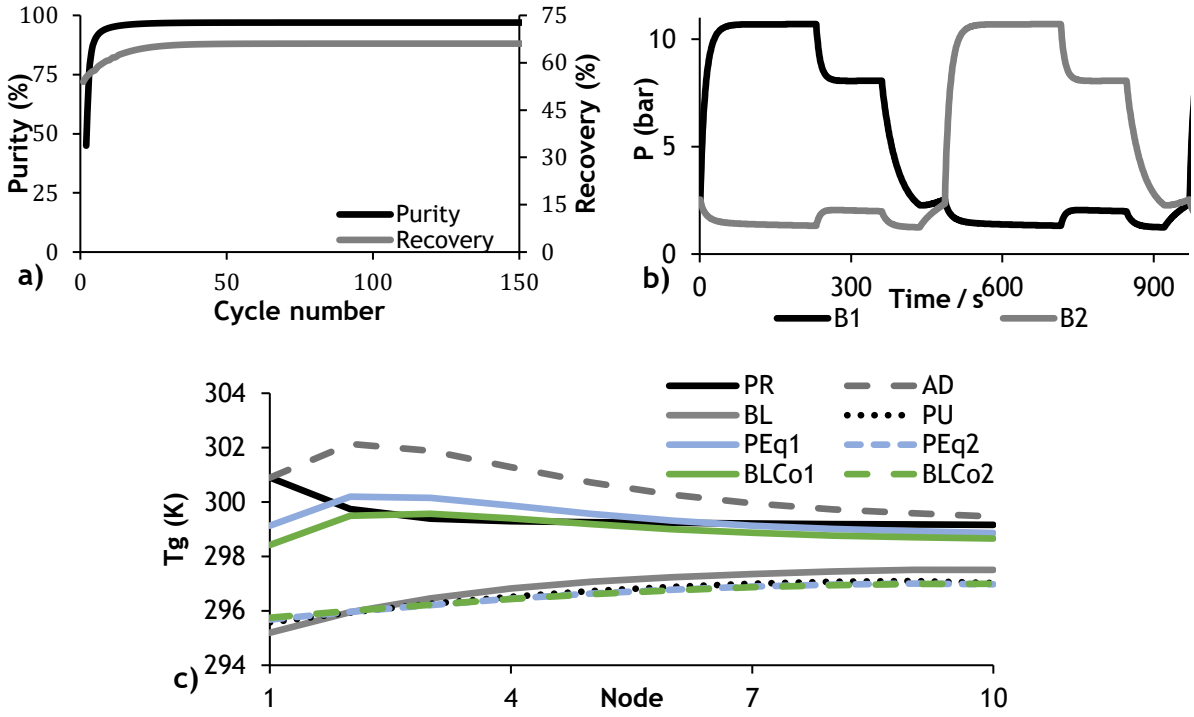


*Figure 19. Simulation results for the 8-step PSA optimized run (8) where: a) evolution of the $CH_4$ purity and recovery with the cycle number; b) pressure obtained at the column outlet at CSS; c) Gas temperature profile along the bed at the end of each step at CSS.*

Additionally, the gas phase and solid phase profiles for both components along the bed at CSS are given in Figure 20. Here, the nitrogen is slightly more strongly adsorbed but the working capacity appears to be the same as that of the last 6-step optimized cycle. Additionally, the difference in the adsorbed amount between each step for methane is slightly increased.

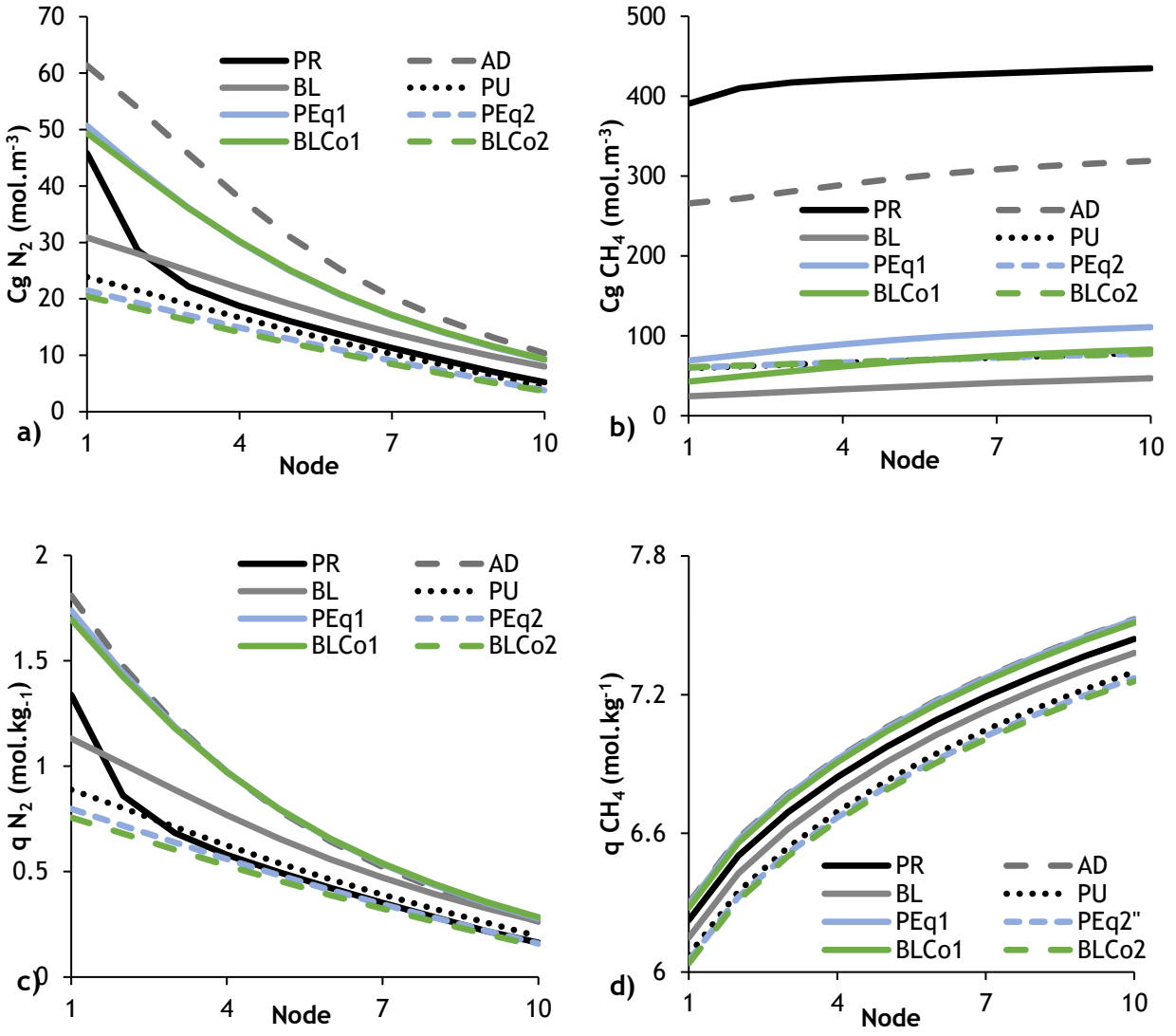


*Figure 20. Gas phase (a and b) and solid phase (c and d) concentration profiles for $N_2$ (a and c) and $CH_4$ (b and d) at CSS obtained for the 8-step PSA optimized run (8).*

### 4.4.4 An improved cycle: VPSA

To improve the previously optimized 6-step cycle a vacuum pump was implemented for the purge step to be operated under vacuum conditions. Therefore, this step cycle is expected to improve the methane recovery while sacrificing the energy consumption.

In order to develop the best cycle able to more effectively regenerate the methane an optimization was developed where the pump set-point was changed (Pump_SP) which is the pressure we want to achieve with the vacuum pump and also the $t_{ads}$. The varied operating parameters as well as the process performance for each array of variables are represented in Table 14. The rest of the parameters are the same as those used in run (11) of the 6-step cycle optimization.

*Table 14. 6-step VPSA optimization variables and process performance for 5 simulations.*

| Run | Pump_SP (bar) | $t_{ads}$ (s) | Purity (%) | Recovery (%) | Productivity ($mol_{CH_4}.kg_{ads}^{-1}.h^{-1}$) |
|---|---|---|---|---|---|
| **(1)** | 0.5 | 100 | 98.35 | 61.57 | 14.4 |
| **(2)** | 0.5 | 150 | 97.57 | 65.62 | 18.9 |
| **(3)** | 0.5 | 200 | 96.92 | 67.85 | 22.4 |
| **(4)** | 0.3 | 220 | 97.19 | 67.86 | 23.6 |
| **(5)** | 0.3 | 250 | 96.85 | 68.65 | 25.3 |

No results for a pump set point lower than 0.3 bar were demonstrated since the process performance would stabilize beyond this point for this cycle configuration. Comparing run (3) with run (4)/(5), the difference in the obtained recovery is not enough to compensate for the higher energetic costs that a pump with an SP of 0.3 bar demands relatively to one with an SP of 0.5 bar. Therefore, the results for the run (3) are exhibited in Figure 21 and Figure 22.

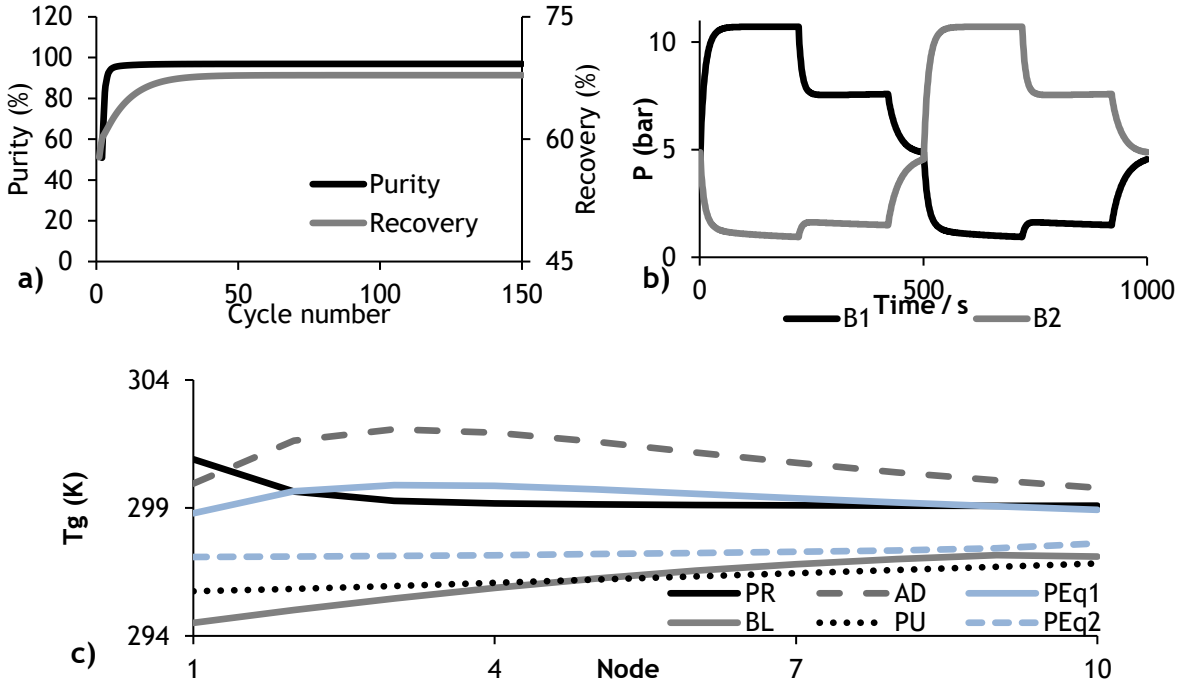


*Figure 21. Simulation results for the 6-step VPSA optimized run (3) where: a) evolution of the $CH_4$ purity and recovery with the cycle number; b) pressure obtained at the column outlet at CSS; c) Gas temperature profile along the bed at the end of each step at CSS.*

It is shown in Figure 21b) that during the blowdown step the pressure drops until sub-atmospheric pressures and during the purge step low pressures are also verified. However, it does not reach the specified set point due to the used CV.

Moreover, the gas phase and solid phase profiles for both components along the bed at CSS, which is achieved after 51 cycles, are given in Figure 22.

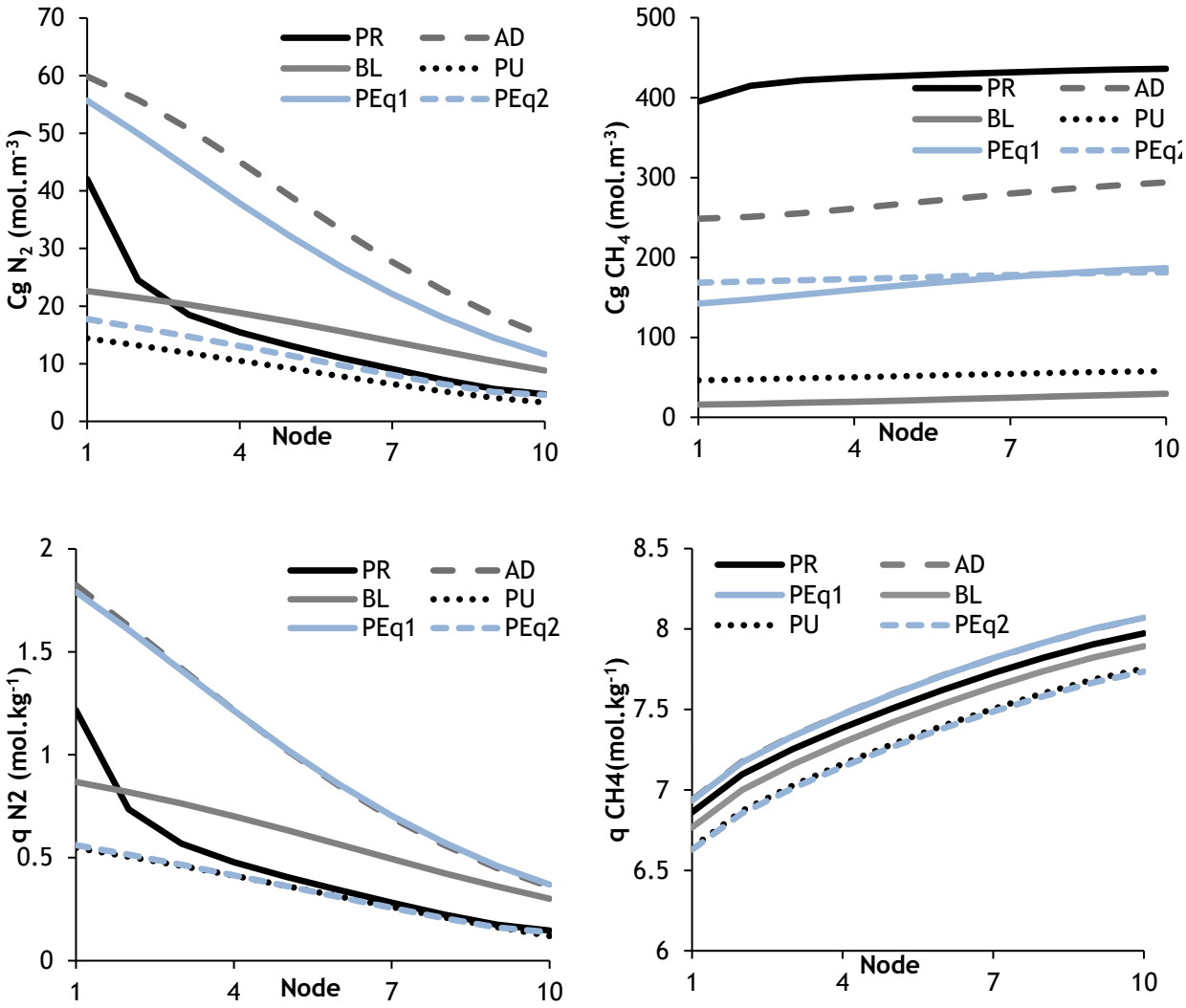


*Figure 22. Gas phase (a and b) and solid phase (c and d) concentration profiles for $N_2$ (a and c) and $CH_4$ (b and d) at CSS obtained for the 6-step VPSA optimized run (3).*

In Figure 22 c) not only the working capacity increased, comparing with previous cycles, but also the adsorption capacity during the adsorption step.

### 4.4.5 8-step cycle VPSA

To combine the best of both upgrades made to the 6-step cycle, an 8-step cycle VPSA was simulated. Furthermore, run (3) from the 6-step VPSA and run (4) from the 8-step PSA were mixed together.

The 2-column apparatus followed the scheme of Figure 18 though the purge step was done at sub-atmospheric pressure. Initially, both columns were filled with nitrogen at the feed

temperature and at 6 bar. The valve's specifications as well as the cycle timetable are displayed in Table 15.

*Table 15. Valves' specifications (.spec) and valve CV coefficient (.CV) if it is applicable for the 8-step VPSA simulation.*

| | PR/BL | AD/PU | BLCo/PU | PEq | BL/PR | PU/AD | PU/BLCo | PEq |
|---|---|---|---|---|---|---|---|---|
| **VF.spec** | 2 | 2 | 2 | 2 | 2 | 2 | 2 | 2 |
| **VF.CV (kmol.s$^{-1}$.bar$^{-1}$)** | $6 \times 10^{-4}$ | | | | | | | |
| **VF1.spec** | 1 | 1 | 0 | 0 | 0 | 0 | 0 | 0 |
| **VF2.spec** | 0 | 0 | 0 | 0 | 1 | 1 | 0 | 0 |
| **VPU.spec** | 0 | 2 | 2 | 2 | 0 | 2 | 2 | 2 |
| **VPU.CV (kmol.s$^{-1}$.bar$^{-1}$)** | $6 \times 10^{-5}$ | | $1 \times 10^{-6}$ | $1 \times 10^{-3}$ | $6 \times 10^{-5}$ | | $1 \times 10^{-6}$ | $1 \times 10^{-3}$ |
| **VP.spec** | 2 | 2 | 2 | 2 | 2 | 2 | 2 | 2 |
| **VP.CV (kmol.s$^{-1}$.bar$^{-1}$)** | $1.5 \times 10^{-4}$ | | | | | | | |
| **VP1.spec** | 0 | 1 | 0 | 0 | 0 | 0 | 0 | 0 |
| **VP2.spec** | 0 | 0 | 0 | 0 | 0 | 1 | 0 | 0 |
| **VW.spec** | 2 | 2 | 2 | 2 | 2 | 2 | 2 | 2 |
| **VW.CV (kmol.s$^{-1}$.bar$^{-1}$)** | $5.7 \times 10^{-4}$ | | | | | | | |
| **VW1.spec** | 0 | 0 | 0 | 0 | 1 | 1 | 1 | 0 |
| **VW2.spec** | 1 | 1 | 1 | 0 | 0 | 0 | 0 | 0 |
| **t (s)** | 230 | 200 | 50 | 30 | 230 | 200 | 50 | 30 |

The simulation performance for the 8-step VPSA with the aforementioned configuration was 97% $CH_4$ purity, 70% $CH_4$ recovery and a productivity of 22.5 $mol_{CH_4}.kg_{ads}^{-1}.h^{-1}$ for which the graphical results are represented in Figure 23 and Figure 24.

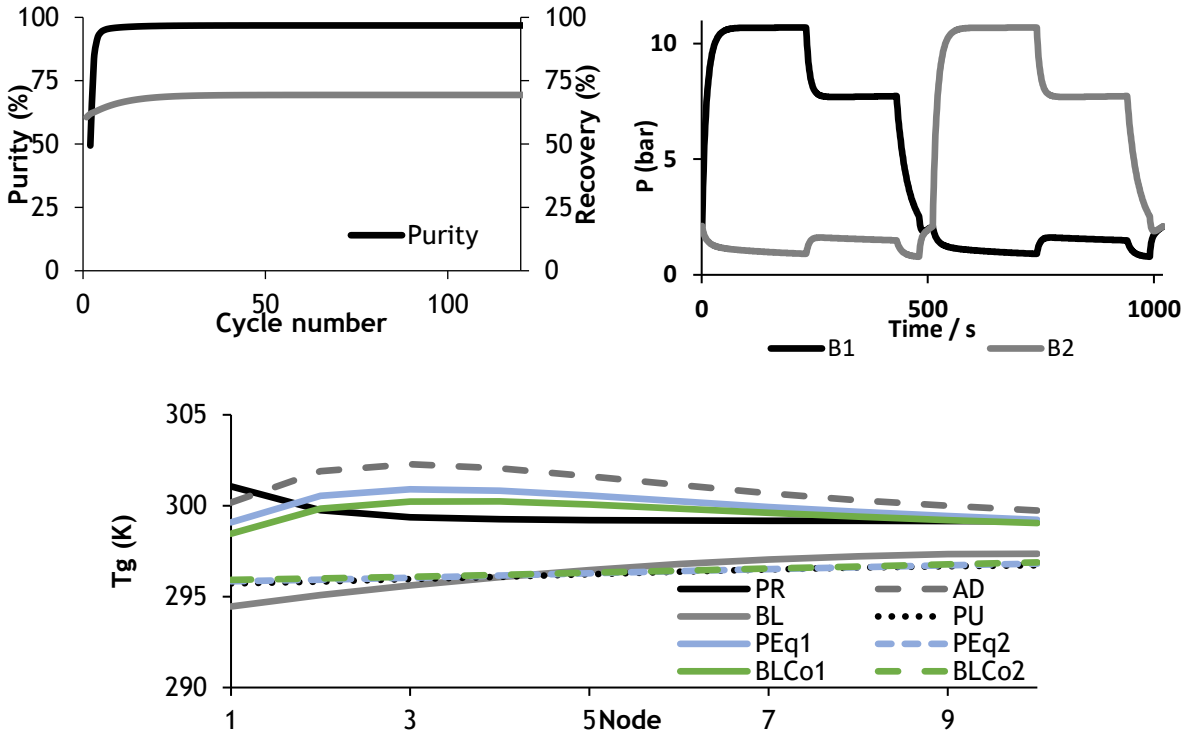


*Figure 23. Simulation results for the 8-step VPSA where: a) evolution of the $CH_4$ purity and recovery with the cycle number; b) pressure obtained at the column outlet at CSS; c) Gas temperature profile along the bed at the end of each step at CSS.*

Furthermore, the gas phase and solid phase profiles for both components along the bed at CSS are given in Figure 24.

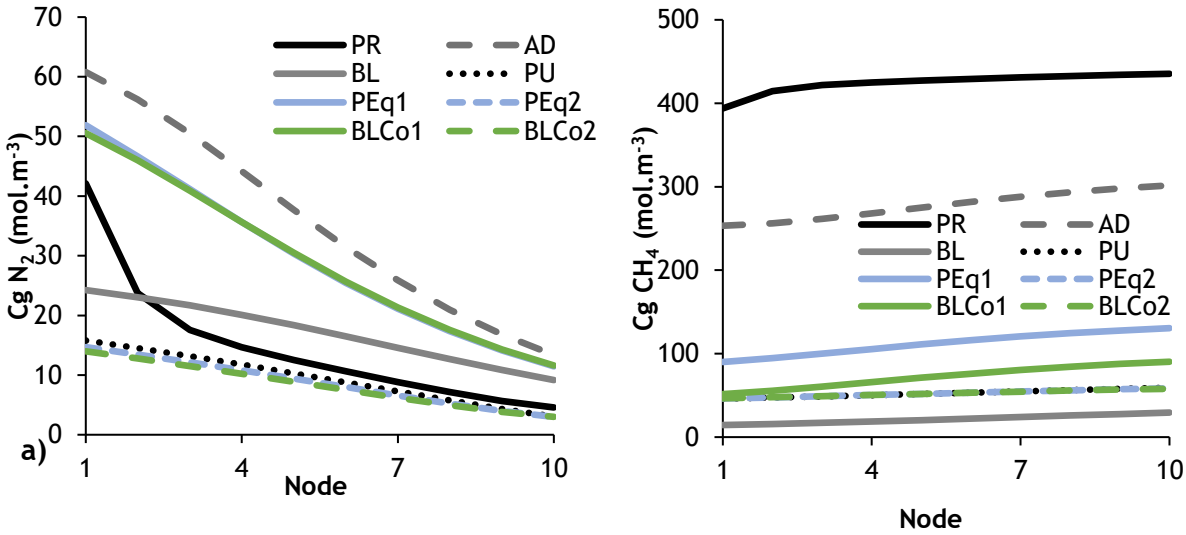

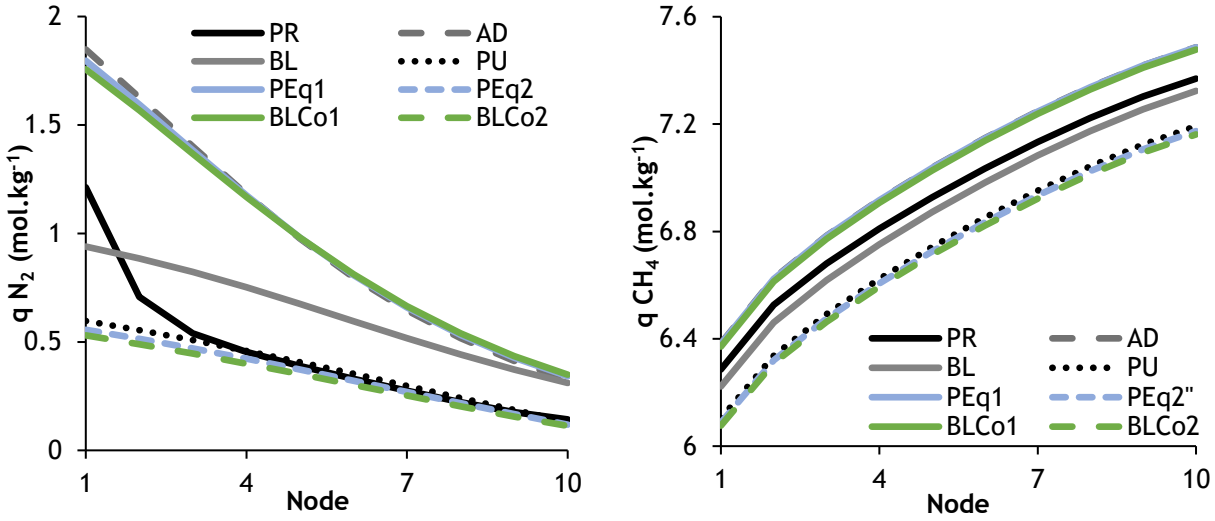


*Figure 24. Gas phase (a and b) and solid phase (c and d) concentration profiles for $N_2$ (a and c) and $CH_4$ (b and d) at CSS obtained for the 8-step VPSA.*

Looking into Figure 24 and comparing it with previous cycles nitrogen solid phases, this cycle configuration demonstrates the best capability to stay well within the bed as it is strongly adsorbed in the CMS but also poorly regenerated. Although there is some considerable variation in the adsorbed amount of $CH_4$ for each step, this difference is higher for $N_2$ so that the overall cycle performance is enhanced.

# 5 Conclusion

The technological concept chosen to overcome the challenges of the removal of $N_2$ from landfill biogas was an adsorption process carried out in a PSA unit with beds filled with either Norit RB-3, an adsorbent selective at equilibrium for $CH_4$ or CMS-3K 172, an adsorbent kinetically selective for $N_2$. The adsorption technology is an interesting economical alternative for landfill gas methane capture with high purity and recovery.

Moreover, the advantages of both adsorbents lie in their commercial availability and reasonable cost, however, the implementation of CMS is desirable owing to unnecessary product recompression. Following the selection of the adsorbent, the equilibrium data was regressed with Langmuir model. The obtained Langmuir parameters were further fitted with the Extended Langmuir 2 equation. The obtained pure equilibrium parameters were used as input in the Aspen Adsorption software and a mathematical model capable of describing the dynamic behavior of multicomponent adsorption in a fixed bed was elaborated.

Subsequently, the industrial PSA design started with an analysis of the simulated breakthrough curves obtained for both adsorbents. For Norit RB-3 pure and binary breakthrough curves were obtained for a flowrate of 500 $Nm^3.h^{-1}$ and a bed dimensioned as D=0.27 m, L=1.37 m and $U_s$=0.23 $m.s^{-1}$ for which the breakthrough point occurred at 23 s and the graphical and predicted $t_{st}$ were, respectively, 33 s and 19 s. The calculated LUB was -0.29 m, a length similar to the used one, validating the bed size estimation. Furthermore, for the CMS, breakthrough curves were attained for several flowrates and a bed dimensioned as D= 0.80 m, L=2.41 m and $U_S$=0.03 $m.s^{-1}$. Within this study, it is inferred that the methane kinetics are extremely slow even though the amount of $CH_4$ that is adsorbed is significative when compared to that of $N_2$. Also, it is shown that a variation of the inlet flowrate will not have a significative impact in the system overall performance. No further work was pursued with the AC adsorbent due to Aspen Adsorption constraints.

The PSA optimization process for the CMS started with a 4-step cycle simulation analysis for a 2-column with the same dimensions as those used in the breakthrough study. The results shown a performance of 97% $CH_4$ purity, 39% $CH_4$ recovery and 4.1 $mol_{CH_4}.kg_{ads}^{-1}.h^{-1}$ productivity at CSS, which is achieved after 217 cycles, that the CV.VP variable as a noticeably impact in the pressure history throughout a cycle and also that the uptake of $N_2$ between the feed and purge step is not significatively different while no variation is verified in methane for each step which implies that there is room for improvement through cycle optimization. The study of the influence of several operational parameters on the process performance revealed that, within

the ranges of parameters values studied, the best overall performance is delivered when varying the VP.CV, for higher purities, and the ratio $U_i/U_{mf}$, for higher recoveries.

Afterwards, two steps were added, namely, two pressure equalizations: 6-step cycle. This new cycle configuration was optimized by testing different sets of operational parameters. The optimized configuration was given for L=1 m, D=0.5 m and a CV.VP of $2\times 10^{-4}$ (kmol.s$^{-1}$.bar$^{-1}$) which delivered a performance of 97.15% $CH_4$ purity, 63.36% $CH_4$ recovery and 14.3 $mol_{CH_4}.kg_{ads}^{-1}.h^{-1}$ productivity at CSS, achieved after 91 cycles. Also, the temperature slightly increases during adsorption and decreases during desorption, the pressure evolution for the used CV.VP is normalized and the working capacity for $N_2$ was increased, as expected, considering the obtained performance.

To enhance the bio-methane recovery, one step was added to the already optimized 6-step cycle, namely, a co-current blowdown after cycle adsorption step: 8-step cycle. After optimization, the attained performance was 96.97% $CH_4$ purity, 66.05% $CH_4$ recovery and 14.5 $mol_{CH_4}.kg_{ads}^{-1}.h^{-1}$ productivity at CSS, achieved after 66 cycles. The solid phase graphics shown that the $N_2$ is slightly more strongly adsorbed in the CMS but the working capacity itself does not significatively varies, when comparing to that of the last cycle.

In addition, to enhance the performance of the optimized 6-step cycle, it was adjusted for a VPSA cycle. The results shown for a pump set point of 0.5 bar were 96.92% $CH_4$ purity, 67.85% $CH_4$ recovery and 22.4 $mol_{CH_4}.kg_{ads}^{-1}.h^{-1}$ productivity at CSS. The solid phase graphics reveal that not only the working capacity increased, comparing with previous cycles, but also the adsorption capacity during the adsorption step.

Finally, to combine the best optimizations, an 8-step cycle VPSA was implemented for a bed with L=1 m, D=0.5 m and a VP.CV of $1.5\times 10^{-4}$ kmol.s$^{-1}$.bar$^{-1}$, among other operational parameters. The simulation performance for the 8-step VPSA was 97% $CH_4$ purity, 70% $CH_4$ recovery and a productivity of 22.5 $mol_{CH_4}.kg_{ads}^{-1}.h^{-1}$. Comparing the obtained solid phase graphic with previous for other cycles, even though there is some considerable variation in the solid loading of $CH_4$ for each step, the difference in the working capacity of $N_2$ and the solid loading of it is so high that the overall performance is enhanced.

Additionally, considering the detected error, the behaviour of methane in terms of its working capacity would be similar to the simulated one. However, since the verified adsorbed amount of methane is much higher than the actual one, and competitive adsorption is being considered, the corrected solid phase results for nitrogen would show a higher working capacity.

# 6 Assessment of the work done

## 6.1 Objectives Achieved

In order to develop a technical concept able to efficiently remove $N_2$ from landfill biogas, the following goals were achieved during the internship:

- Selection of the technology adequate for this separation;
- Selection of the adsorbent and its equilibrium and kinetics study;
- Understanding of the functioning of Aspen Adsorption software;
- Development of a PSA unit with a kinetically selective adsorbent towards $N_2$ according to the given specifications;
- Progressive optimization of the PSA configurations to try to achieve the requirements of the end-product.

Even though the end-product requirements were not achieved, the work done has a huge margin of progress as well as potential to overcome the challenges of this separation.

## 6.2 Limitations and Future Work

Throughout the developed work, the main limitations were the complexity of the software and its several critical details. The understanding of such details and how the software simulates the physical phenomena of adsorption was highly time-consuming and, therefore, limited the further optimization of the developed PSA unit.

Further work should comprehend the input of the proper pure equilibrium data for a 4-step PSA and its progressive optimization. Perhaps, the implementation and optimization of a Dual-Reflux PSA would also be a good option to achieve higher system recoveries.

Regarding DMT, the employment of a pilot installation at a laboratorial scale to conduct practical studies of the adsorbent's equilibrium and kinetics as well as to accurately test different operational parameters of the PSA unit would be beneficial by offering to the company the autonomy to develop PSA applications without the need of external partnerships.

## 6.3 Final Assessment

The developed project was very enriching, personally, since it allowed the understanding of a new software and a deeper comprehension of the phenomena happening behind a PSA. This work provides crucial information and simulations for the development of a PSA unit able to remove nitrogen from landfill biogas in order to produce bio-methane with high purity as well as recovery.

# 7 References


1. UN, *Adoption of the Paris Agreement*. 2015.
2. Steinhauser, D.D.a.A., *Biogas from Waste and Renewable Resources*. Wiley-VCH, 2008.
3. Delgado, J.A., et al., *Simulation of the recovery of methane from low-concentration methane/nitrogen mixtures by concentration temperature swing adsorption*. Separation and Purification Technology, 2019. **209**: p. 550-559.
4. EPA, *Understanding Global Warming Potentials*. 2020.
5. WBA, *World Potential of Biogas*. 2019.
6. Grande, C.A., *Biogas upgrading by pressure swing adsorption*. Biofuel's engineering process technology, 2011: p. 65-84.
7. Monteiro, E., V. Mantha, and A. Rouboa, *Prospective application of farm cattle manure for bioenergy production in Portugal*. Renewable Energy, 2011. **36**(2): p. 627-631.
8. IEA, *Outlook for biogas and biomethane: Prospects for organic growth*. 2020: Paris.
9. Hinge, L.B.A.a.J., *Biogas and bio-syngas upgrading*. 2012, Danish Technological Institute: Aarhus.
10. Mokhatab, S., W.A. Poe, and J.Y. Mak, *Chapter 4 - Basic Concepts of Natural Gas Processing*, in *Handbook of Natural Gas Transmission and Processing (Fourth Edition)*, S. Mokhatab, W.A. Poe, and J.Y. Mak, Editors. 2019, Gulf Professional Publishing. p. 177-189.
11. Li, Z., *Separation of Nitrogen from Natural Gas: Conventional and Emerging Technologies*, in *Fluid Sciences and Resources Divisionn*. 2018, The University of Western Australia.
12. Rufford, T.E., et al., *The removal of CO2 and N2 from natural gas: A review of conventional and emerging process technologies*. Journal of Petroleum Science and Engineering, 2012. **94**: p. 123-154.
13. Yang, R.T., *Adsorbents: fundamentals and applications*. 2003: John Wiley & Sons.
14. Baker, R.W. and K. Lokhandwala, *Natural Gas Processing with Membranes: An Overview*. Industrial & Engineering Chemistry Research, 2008. **47**(7): p. 2109-2121.
15. Echterhoff, L. and V. Pathak, *Evaluation of process costs for small-scale nitrogen removal from natural gas. Topical report, January 1989-December 1989*. 1991, Pullman Kellogg.
16. Grande, C.A., *Advances in pressure swing adsorption for gas separation*. International Scholarly Research Notices, 2012. **2012**.
17. Castle, W., *Air separation and liquefaction: recent developments and prospects for the beginning of the new millennium*. International Journal of Refrigeration, 2002. **25**(1): p. 158-172.
18. Abdeljaoued, A., et al., *Simulation and experimental results of a PSA process for production of hydrogen used in fuel cells*. Journal of environmental chemical engineering, 2018. **6**(1): p. 338-355.
19. Samanta, A., et al., *Post-combustion CO2 capture using solid sorbents: a review*. Industrial & Engineering Chemistry Research, 2012. **51**(4): p. 1438-1463.

20. Saleman, T.L., et al., *Capture of low grade methane from nitrogen gas using dual-reflux pressure swing adsorption.* Chemical Engineering Journal, 2015. **281**: p. 739-748.

21. Xiao, G., et al., *Nitrogen rejection from methane using dual-reflux pressure swing adsorption with a kinetically-selective adsorbent.* Chemical Engineering Journal, 2019. **372**: p. 1038-1046.

22. Li, J.-R., R.J. Kuppler, and H.-C. Zhou, *Selective gas adsorption and separation in metal–organic frameworks.* Chemical Society Reviews, 2009. **38**(5): p. 1477-1504.

23. Broom, D., *Characterizing adsorbents for gas separations.* Chem. Eng. Prog, 2018. **114**: p. 30-37.

24. Lu, W., et al., *Rejecting N2 from natural gas by dual reflux pressure swing adsorption with activated carbon.* Journal of Natural Gas Science and Engineering, 2020. **81**: p. 103457.

25. Effendy, S., C. Xu, and S. Farooq, *Optimization of a pressure swing adsorption process for nitrogen rejection from natural gas.* Industrial & Engineering Chemistry Research, 2017. **56**(18): p. 5417-5431.

26. Yoon, J.W., et al., *Selective nitrogen capture by porous hybrid materials containing accessible transition metal ion sites.* Nature materials, 2017. **16**(5): p. 526-531.

27. Rufford, T.E., et al., *Adsorption equilibria and kinetics of methane+ nitrogen mixtures on the activated carbon Norit RB3.* Industrial & Engineering Chemistry Research, 2013. **52**(39): p. 14270-14281.

28. Mitariten, M. *Nitrogen removal from natural gas with the molecular gate adsorption process.* in *88th Annual Convention of the Gas Processors Association*. 2009.

29. Saleman, T., et al., *A robust dynamic column breakthrough technique for high-pressure measurements of adsorption equilibria and kinetics.* Adsorption, 2017. **23**(5): p. 671-684.

30. Waldron, W. and S. Sircar, *Parametric study of a pressure swing adsorption process.* Adsorption, 2000. **6**(2): p. 179-188.

31. Ruthven, D.M. and F. Pressure, *Swing Adsorption.* New York: VCH Publishers, 1994. **1**(994): p. 235.

32. Salehi, R.N., F. Rahimpour, and S. Sharifnia, *Adsorption of carbon dioxide, nitrogen and methane on modified titanosilicate type molecular sieves.* Journal of Natural Gas Science and Engineering, 2017. **46**: p. 730-737.

33. Kuznicki, S.M., et al., *Small-pored crystalline titanium molecular sieve zeolites and their use in gas separation processes.* 2000, Google Patents.

34. Dolan, W.B. and K.F. Butwell, *Selective removal of nitrogen from natural gas by pressure swing adsorption.* 2002, Google Patents.

35. Cavenati, S., et al., *Adsorption of small molecules on alkali-earth modified titanosilicates.* Microporous and Mesoporous Materials, 2009. **121**(1-3): p. 114-120.

36. Guild Associates, I. *Molecular Gate Adsorbent Technology.* 2020 27 october 2020]; Available from: https://www.guildassociates.com/MGTech.

37. Creutz, S.E. and J.C. Peters, *Catalytic reduction of N2 to NH3 by an Fe-N2 complex featuring a C-atom anchor.* Journal of the American Chemical Society, 2014. **136**(3): p. 1105-1115.

38. Yang, R.T., *Gas separation by adsorption processes.* Vol. 1. 1997: World Scientific.

39. Langmuir, I., *The adsorption of gases on plane surfaces of glass, mica and platinum.* Journal of the American Chemical society, 1918. **40**(9): p. 1361-1403.

40. Hu, G., et al., *Enrichment of low grade CH4 from N2/CH4 mixtures using vacuum swing adsorption with activated carbon*. Chemical Engineering Science, 2021. **229**: p. 116152.

41. McCabe, W.L., J.C. Smith, and P. Harriott, *Unit operations of chemical engineering*. Vol. 5. 1993: McGraw-hill New York.

42. Seader, J.D., E.J. Henley, and D.K. Roper, *Separation process principles*. Vol. 25. 1998: wiley New York.

43. Cavenati, S., C.A. Grande, and A.E. Rodrigues, *Separation of methane and nitrogen by adsorption on carbon molecular sieve*. Separation Science and Technology, 2005. **40**(13): p. 2721-2743.

44. Xiao, G., et al., *Adsorption equilibria and kinetics of CH 4 and N 2 on commercial zeolites and carbons*. Adsorption, 2017. **23**(1): p. 131-147.

45. Qi, W., M. Wang, and Q. Liu, *Shape factor of nonspherical nanoparticles*. Journal of materials science, 2005. **40**(9-10): p. 2737-2739.

46. Zhang, Y., et al., *Non-isothermal numerical simulations of dual reflux pressure swing adsorption cycles for separating N2+ CH4*. Chemical Engineering Journal, 2016. **292**: p. 366-381.

47. Ruthven, D.M., *Principles of adsorption and adsorption processes*. 1984: John Wiley & Sons.

48. Aspen Technology, *Aspen Adsim 2004.1, Adsorption Reference Guide*. 2005.

49. Duong, D., *D. Adsorption Analysis: Equilibria and Kinetic*. Imperial College Piss London, 1998: p. 156.

50. McDonald, R.P. and M.-H.R. Ho, *Principles and practice in reporting structural equation analyses*. Psychological methods, 2002. **7**(1): p. 64.

51. Wood, K.R., Y.A. Liu, and Y. Yu, *Design, Simulation and Optimization of Adsorptive and Chromatographic Separations: A Hands-On Approach*. 2018.

52. Carberry, J.J., *Chemical and catalytic reaction engineering*. 2001: Courier Corporation.

53. Narin, G., et al., *Propylene/nitrogen separation in a by-stream of the polypropylene production: from pilot test and model validation to industrial scale process design and optimization*. Industrial & Engineering Chemistry Research, 2014. **53**(22): p. 9199-9213.

54. Loureiro, J.M., *Apontamentos Estrasburgo*.

# Appendix A – Biogas specifications according to its source and Natural Gas grid requirements

*Table 1. Average composition of biogas according to its sources and comparison with the natural gas pipeline requirements in both the USA and the Netherlands.*

| **Biogas Source** | Landfill [1] | Agricultural/Food industries [1] | Sewage Sludge [1] | **Natural Gas pipeline requirements** | USA (state of Oregon) [2] | Netherlands [1] |
|---|---|---|---|---|---|---|
| **$CH_4$** | 40-80% | 50-70% | 50-80 | | - | - |
| **$N_2$** | 15-20% | 0-1% | 0-3% | | <2.75% | 14% |
| **$CO_2$** | 15-40% | 30-50% | 20-50% | | 2% | 0.2-1.5% |
| **$O_2$** | 1% | 0-1% | 0-1% | | - | - |
| **$H_2$** | 0-3% | 0-2% | 0-5% | | - | - |
| **$NH_3$** | 5 ppm | 50-100 mg/$m^3$ | Vestigial traces | | - | - |
| **$H_2O$ (vapour)** | Saturated | Saturated | | | - | - |
| **CO** | - | 0-1% | 0-1% | | - | - |
| **$H_2S$** | 0-100 ppm | 100-700 ppm | 0-1% | | - | - |
| **Siloxanes** | 0-50 $mg.m^{-3}$ | Not reported | 0-100 $mg.m^{-3}$ | | - | - |

**References:**

1. Awe, O., et al., A Review of Biogas Utilisation, Purification and Upgrading Technologies. Waste and Biomass Valorization, 2017. 8.

2. World, B., Biomethane Market Intelligence Report. 2020.

# Appendix B – Physical and chemical properties of nitrogen and methane

*Table 1. List of physical and chemical properties of nitrogen and methane.*

| **Physical Properties** | | |
|---|---|---|
| | $N_2$ | $CH_4$ |
| **Kinetic Diameter (Å)** | 3.64 | 3.80 |
| **Normal Boiling Point (NBP) (K)** | 77.3 | 111.7 |
| **Critical Temperature (K)** | 126.2 | 3.80 |
| **Critical Pressure (kPa)** | 3400 | 4600 |
| **$\Delta H_{vap}$ at NBP (KJ/mol)** | 5.58 | 8.17 |
| **Polarisability ($Å^3$)** | 1.710 | 2.448 |
| **Dipole moment (D)** | 0 | 0 |
| **Quadrapole Moment (D Å)** | 1.54 | 0.02 |
| **Chemical Properties** | | |
| **Methane valorization through chemical conversion onto significant products** | | |
| **$CH_4$ conversion to methanol** | $CH_4 + \frac{1}{2}O_2 \rightarrow CH_3OH$ | (1) |
| **Oxidative coupling of $CH_4$** | $2CH_4 + \frac{1}{2}O_2 \rightarrow CH_3CH_3 + H_2O$ | (2) |
| **$CH_4$ steam reforming** | $CH_4 + H_2O \rightarrow CO + 3H_2$ | (3) |
| **Nitrogen fixation reactions** | | |
| **Biological $N_2$ fixation by nitrogenase** | $N_2 + 16ATP^{2-} + 8H^+ \rightarrow 2NH_3 + 16ADP^- + 16H_2PO_4^- + H_2$ | (4) |
| **Reversible $N_2$ bonding on TMC at high temperature and pressure** | $N_2 + TMC \rightarrow N_2 * TMC$ | (5) |
| **$N_2$ fixation by Haber-Bosch process, with a catalyst** | $N_2 + 3H_2 \rightarrow 2NH_3$ | (6) |
| **Electrochemical $N_2$ fixation** | $N_2 + 3H_2 \rightarrow 2NH_3$ | (7) |
| **$N_2$ fixation by a lithium metal** | $N_2 + 6Li \rightarrow 2Li_3N$ | (8) |

# Appendix C – Emerging technologies for the separation of $N_2$ and $CH_4$

1. Biological Nitrogen Fixation (BNF)

This biological nitrogen fixation (BNF) naturally occurs when molecular nitrogen present in the air is captured and converted to fertilizer by some microorganisms. BNF can occur under ATM (atmospheric) conditions due to the high catalytic ability of nitrogenase, the bio-catalyst for BNF. Currently, there are various types of nitrogenase enzymes with different metal cofactors, while molybedenium-iron complex is the most common example [1]. As seen in equation (1) to reduce $N_2$ are required 8 electrons and 16 adenosine triphosphate (ATP).

This process offers an opportunity to capture nitrogen from natural gas, in a green way, under moderate conditions. Nonetheless, the nitrogen capacity on nitrogenase and FeMo cofactor are extremely low, respectively, 0.0029 and 0.7168 $mol.kg^{-1}$. These are too small compared to the reported adsorbents and, therefore, cannot meet the requirements to become an industrial process. Also, the scarcity of its sources [2] and the demanded energetic consumtion are decisive factors in excluding this method for this separation.

2. Transitional Metal Complex (TMC) process

TMC is a bulky molecule with a central transition metal ion and several supporting ligands. It is named transition metal due to its partially filled electron sub-shell [3]. Also, ligands are ions or anionic molecules that bind to the metal center, sharing their electron density.

Nitrogen can bind to TMC in several different modes although the most relevant for the removal of nitrogen from methane is called mononuclear end-on, as seen in figure 1. It involves a σ-donation from the lone electron pairs of nitrogen molecule to the empty $d_{z2}$ or $d_{x2-y2}$ orbitals of the metal centre and a back-$\pi$-donation from the filled $d_{xz}$, $d_{yz}$ or $d_{xy}$ orbitals of metal centre to the vacant $\pi^*$ orbitals of nitrogen molecule [4].

*Figure 1- End-on bonding mode [4].*

Unlike nitrogen, methane does not exhibit additional lone pairs of electrons to form a σ bond with the TMC or an empty π* orbital to accept electrons from the TMC to form a π back-bond. Hence, this is a determinative factor that can be exploited to develop a separation process that captures nitrogen from methane [5]. An interesting example of TMC application is as a TMC-polymer-solvent combination in the Cr-Mil, a metal organic framework adsorbent, which was

demonstrated to have improved nitrogen capacities [6]. TMC based processes may also be applied to absorption, with proven enhanced properties relatively to the traditional process.

TMC based processes are a promising but under-developed technology with the potential to meet the criteria presented in Chapter 2.3 to be considered for the separation of nitrogen and methane.

3. Haber-Bosch Process

Haber-Bosch is a well-established process which produces more than 150 million tons of ammonia from nitrogen and hydrogen every year [7]. The possibility of capturing nitrogen from biogas streams and converting it to ammonia, a valuable product, is worth the attention.

However, this is a process tricky to adjust for this separation, due to scaling down necessities and exceedingly different operational conditions. Also, it is energetically intensive and raises some safety concerns.

4. Electrochemical nitrogen fixation

Resembling the TMC-based process, an alternative electrochemical route has emerged with the potential to reduce the energy consumption of the Haber-Bosch process by 20% [8]. Likewise, this process reduces nitrogen from biogas streams to ammonia, but electrochemically, with an electrolytic cell, composed of two electrodes, the anode and the cathode and electrolytes in the middle as seen in Figure 2.

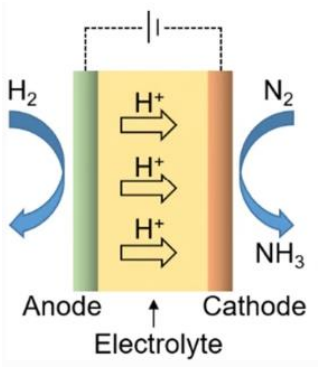


*Figure 1- Illustration of the electrochemical process of the reduction of nitrogen to ammonia [9].*

Overall, its functioning is based on the application of an external voltage, which forces hydrogen to lose his electrons, generating protons which are directed to the cathode, where they contact with the biogas stream and react with nitrogen to produce ammonia. Furthermore, ammonia can easily be separated from methane due to their different volatilities.

Xu et al. reported the highest ammonia production rate of $1.13\times 10^{-8}$ mol.cm$^{-2}$.s$^{-1}$ with a current efficiency of 90 %, achieved with a Nafion membrane 102 as the electrolyte. However

good the prospects of the development of this technology are for this specific application, it requires maturation. The capital cost of electrolyte is already too far elevated to make it economically feasible, even without mentioning the anode and cathode. Also, the real ammonia production rate is quite different from the theoretical one and by the analysis of the required areas, there is the need to scale up the process which would impose some difficulties.

5. Lithium based process

Over the years, lithium has been mentioned as a possible energy carrier. Basically, lithium reacts with nitrogen originating $Li_3N$, under a moist atmosphere at moderate conditions [10].

In 1990, a process to exclude lithium from crude argon was assembled with a nitrogen removal unit containing lithium either supported on high surface area materials or in a molten state for a temperature range of 100 to 200 °C, converting the nitrogen into lithium nitride [11]. A similar process could be adapted for the removal of nitrogen from natural gas operating in a batch mode which is akin to a pressure or temperature swing adsorption process. Theoretically, the loading capacity of nitrogen on lithium is 24 $mmol.g^{-1}$, which constitutes an advantage to other conventional adsorbents. The selectivity for nitrogen is also considerably high since the lithium does not react with methane, originating an end product with a full recovery of methane. Therefore, the utilization of lithium to remove nitrogen is a potential candidate for the mentioned separation due to its scalability, safety and efficiency [12].

Nonetheless, the process requires some developments to become feasible, namely, the need for the reaction to occur under moderate temperatures and also the regeneration of the lithium metal from $Li_3N$, which might need many harsh conditions.

**References:**

1. Gilbertson, J.D., et al., Coordination chemistry of H2 and N2 in aqueous solution. Reactivity and mechanistic studies using trans-FeII (P2) 2X2-type complexes (P2= a chelating, water-solubilizing phosphine). Inorganic chemistry, 2007. 46(4): p. 1205-1214.

2. Petroleum, B., BP statistical review of world energy 2017. Br. Pet, 2017. 66: p. 1-52.

3. McNaught, A.D. and A. Wilkinson, Compendium of chemical terminology. Vol. 1669. 1997: Blackwell Science Oxford.

4. Fryzuk, M.D. and S.A. Johnson, The continuing story of dinitrogen activation. Coordination Chemistry Reviews, 2000. 200: p. 379-409.

5. Thorneley, R.N. and D.J. Lowe, Kinetics and mechanism of the nitrogenase enzyme system. Molybdenum enzymes, 1985. 7: p. 89-116.

6. Koros, W.J. and C. Zhang, Materials for next-generation molecularly selective synthetic membranes. Nature materials, 2017. 16(3): p. 289-297.

7. Hazari, N., Homogeneous iron complexes for the conversion of dinitrogen into ammonia and hydrazine. Chemical Society Reviews, 2010. 39(11): p. 4044-4056.

8. Andersen, S.Z., et al., A rigorous electrochemical ammonia synthesis protocol with quantitative isotope measurements. Nature, 2019. 570(7762): p. 504-508.

9. Li, C., T. Wang, and J. Gong, Alternative Strategies Toward Sustainable Ammonia Synthesis. Transactions of Tianjin University, 2020. 26(2): p. 67-91.

10. Besson, J. and W. Muller, THE REACTION OF NITROGEN WITH LITHIUM AT ORDINARY TEMPERATURE AND THE ROLE OF WATER VAPOR IN THIS REACTION. Compt. rend., 1958. 247.

11. Joshi, A.V., Inert gas purification. 1995, Google Patents.

12. Li, Z., Separation of Nitrogen from Natural Gas: Conventional and Emerging Technologies, in Fluid Sciences and Resources Divisionn. 2018, The University of Western Australia.

# Appendix D - Membrane Technology: Types of membranes

Membranes can be sub-divided into three types, according to the material composition: polymer membranes which can either be $CH_4$ selective (rubbery polymer membrane) or $N_2$ selective (glass polymer membrane); mixed matrix membranes which are adapted to be $CH_4$ or $N_2$ selective; inorganic molecular sieve membranes that have been developed to be impermeable for $N_2$. A membrane performance is usually evaluated by their permeance and separation selectivity *a* [1].

The polymer membranes usually display low selectivities for both components, an obstacle possible to overcome through multi-stage process design. By now, the NitroSep$^{TM}$ membrane is the only methane selective membrane technology to be industrially implemented. The technology is a two-stage membrane unit able to process up to 30 000 $Nm^3.h^{-1}$, with a $CH_4$ recovery of 93% for a biogas feed with a $N_2$ content lower than 12%. However, the process becomes economically impractical for biogas streams with over 30% of nitrogen. Simulation studies regarding these membranes have shown that a selectivity of nitrogen over methane of 17 is demanded to treat flowrates with 10% of nitrogen in order to meet pipeline specifications [2]. So far, the best performance comes with a selectivity of 2.3, for a glass polymer membrane [3]. Additionally, these membranes are quite sensitive to high pressure flows and the presence of contaminants in the biogas stream, resulting in their plasticization and swelling.

Inorganic membranes, in contrast with the polymer ones, can achieve higher selectivities and nitrogen permeances. Nonetheless, these membranes industrial production without flaws is intangible due to the needed rigorous porous structure demand to achieve such selectivities [4]. To address this issue, carbon molecular sieves (CMS) membranes prepared from polymer precursors through pyrolysis are under study [5].

The purpose of the mixed matrix membranes is to integrate the inorganic molecular sieves into a polymer matrix, combining the pluses of each and delivering a product with the desired separation performance as well as the robust and flexible mechanical properties. However, the practicability of this technology is still a challenge due to the poor compatibility among them [6].

**References:**

1. Carreon, M.A., Molecular sieve membranes for N2/CH4 separation. Journal of Materials Research, 2018. 33(1): p. 32-43.

2. Baker, R.W. and K. Lokhandwala, Natural Gas Processing with Membranes: An Overview. Industrial & Engineering Chemistry Research, 2008. 47(7): p. 2109-2121.

3. Tanaka, K., et al., Permeability and permselectivity of gases in fluorinated and non-fluorinated polyimides. Polymer, 1992. 33(3): p. 585-592.

4. Ning, X. and W.J. Koros, Carbon molecular sieve membranes derived from Matrimid® polyimide for nitrogen/methane separation. Carbon, 2014. 66: p. 511-522.

5. Koros, W.J. and C. Zhang, Materials for next-generation molecularly selective synthetic membranes. Nature materials, 2017. 16(3): p. 289-297.

6. Li, Z., Separation of Nitrogen from Natural Gas: Conventional and Emerging Technologies, in Fluid Sciences and Resources Divisionn. 2018, The University of Western Australia.

# Appendix E - Other Skarstrom modifications

1. Backfilling column

This step is considered to ensure a high purity of the final product. It consists of a pressurization, at counter current, of the column preparing to be pressurized with part of the final product, allowing the creation of a higher concentration gradient of the light component at the top. This factor prevents non-adsorbed heavy components from leaving the column during the feed step [1].

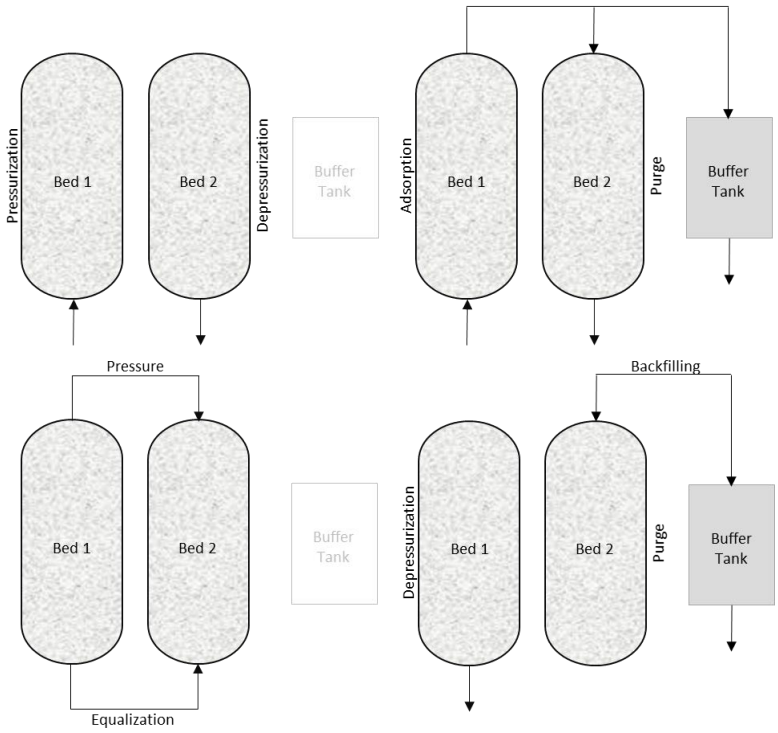


*Figure 1. Modified Skarstrom half-cycle with both equalizing pressure and backfilling step. Adapted from [2].*

2. Rinse step

This Rinse/Washing stage of the saturated column occurs after the adsorption step and is capable of improving product recovery when the light component adsorption is similar to the one of the heavy component (close or low selectivities). The column regeneration with a saturated current of the heavier component allows a much more effective desorption of the light component in the column significatively improves the ending product recovery [2].

3. Dual Reflux Pressure Swing Adsorption

Dual-reflux (DR) PSA is an innovative cycle which uses dual-reflux streams to enhance the performance of the conventional Skarstrom cycle, specifically, the enrichment and, theoretically, it is capable of a perfect separation with any bed pressures [3].

Conventional adsorption processes have demonstrated some constraints with the production of two products with useful purity, particularly when the selectivity of the more adsorbed component, over the light component is modest. This is aggravated when the feed concentration of the heavy component is relatively low. DR PSA emerges with the advantage of an increased separation power for a given adsorbent through the use of simultaneous heavy and light reflux streams [4].

The feed stream enters in the middle of the column, while light and heavy product streams are drawn from the bottom and top of each bed, respectively. The implementation of a simultaneous heavy component reflux bed increases its local pressure in the pressurized column relative to that in the feed which implies that the enrichment is not limited by the ratio of bed pressures. In its place, material balance constraints occur, diminishing the theoretical boundaries of the two product's purities and, under many conditions, it is actually possible to achieve two pure products.

4. Multi-layer adsorbent

Often, it is rewarding to display in an adsorption bed different adsorbents with different properties, properly displayed in multilayers since PSA technology is a dynamic process where the mixture to be separated varies in every stage of the column. As the concentration front advances, the molar fraction of the lighter component in the inter-particular phase increases and, therefore, the inlet mixture to be separated at the "first section" of the bed is completely different from the one at the "final stage". Hence, since the separation is completely different so should be the adsorbent.

A major advantage of using a kinetic adsorbent such as MSC-3K is that it usually exhibits an average balance between purity and recovery and consumes less power than others. The main disadvantage is that the equilibrium capacity is extremely low because the process is controlled kinetically and the length of the mass transfer zone is comparable or even larger than the length of the columns. In order to adjust the properties of the bed without changing the adsorbent, two or more layers of different adsorbents may be applied to enhance the unit productivity and power consumption for biogas upgrading. To address this matter, after a layer of a kinetically selective adsorbent, an equilibrium selective one could be implemented.

The application constraints of this method to this separation are the fact that there is a lack of equilibrium selective adsorbents for nitrogen over methane if the goal is to adsorb the nitrogen to diminish the energy consumption costs [5].

**References:**

1. Liow, J.L. and C. Kenney, The backfill cycle of the pressure swing adsorption process. AIChE journal, 1990. 36(1): p. 53-65.

2. Yang, R.T., Gas separation by adsorption processes. Vol. 1. 1997: World Scientific.

3. Saleman, T.L.H., Adsorption-based separations of gaseous nitrogen and methane mixtures. School of Mechanical and Chemical Engineering, 2016.

4. Lu, W., et al., Rejecting N2 from natural gas by dual reflux pressure swing adsorption with activated carbon. Journal of Natural Gas Science and Engineering, 2020. 81: p. 103457.

5. Liu, Z., et al., Multi-bed vacuum pressure swing adsorption for carbon dioxide capture from flue gas. Separation and Purification Technology, 2011. 81(3): p. 307-317.

# Appendix F - Comparison of the technologies for the removal of $N_2$ from $CH_4$

*Table 1. Comparison study of all the mentioned technologies for the removal of nitrogen from natural gas.*

| | Membranes | | | Cryogenic Distillation | Adsorption | | Absorption | |
|---|---|---|---|---|---|---|---|---|
| | **Polymer** | **Inorganic** | **Mixed Matrix** | | **$CH_4$ selective** | **$N_2$ selective** | **$CH_4$ selective** | **$N_2$ selective** |
| **Maturation** | Well-established | Upgrading | Early stage | Well-established | Well-established but there is a lack of proper adsorbents, especially for $N_2$ | | Well-established | No further investigation since 1960 |
| **Gas Processing scale** | Possible scale-up | Hard to scale-up | Hard to scale-up | Cost prohibitive for flows >17 000 $Nm^3.h^{-1}$ with high capital and operational costs | Scalable but, for this separation, only flows <16 000 $Nm^3.h^{-1}$ | | 2000 to 30000 $Nm^3.h^{-1}$ | Adaptable |
| **Capital and operational costs** | Inexpensive technology | | | | Cheap technology but higher costs with recompression if it´s $CH_4$ selective | | Energy intensive | |
| **Separation Performance** | Low performance | Reasonable performance | Promising better performance | High purities and recoveries | Promising performance dependent on adsorbents and PSA development | | Low performance | |
| **Safety** | Safe | | | Safety issues | Safe | | Safe | Dangerous |
| **Equilibrium selectivity** | 2-3 when $N_2$ selective and 0.25 to 0.3 when $CH_4$ selective | | | 5-8 | 0.25-0.5 | 1.3-2 | - | - |
| **Separation power** | 2-10 | | | 320 | 1.3-2 | 8-40 | - | - |

$$\alpha'_{i,j} = \frac{x_i / y_i}{x_j / y_j} \quad (1)$$

$$SP_{i,j} = \frac{C_i^a / C_i^b}{C_i^a / C_j^b} \quad (2)$$

This equilibrium selectivity is defined in terms of phase concentration and the one mentioned in Equation (1) in page 8 is specific for adsorption processes. Whereas, here in Equation (1), a broader concept of this factor, $x_i$ and $x_j$ are the mole fractions at a first equilibrium phase and $y_i$ and $y_j$ represent the same as before but in a secondary equilibrium phase.

Furthermore, in equation (2), $C_i^1$ and $C_j^1$ are the concentrations at the product stream *a* while $C_i^2$ and $C_j^2$ are the concentrations at the product stream *b* [1].

**References:**

1. Rufford, T.E., et al., The removal of CO2 and N2 from natural gas: A review of conventional and emerging process technologies. Journal of Petroleum Science and Engineering, 2012. 94: p. 123-154.

# Appendix G - Comparison of the different adsorbents' performance

*Table 1. Selectivities for $N_2$ over $CH_4$ for different adsorbents and the respective commercial distributor.*

| Type | Adsorbent | $N_2/CH_4$ Equilibrium Selectivity | $N_2/CH_4$ Kinetic Selectivity | Temperature (K) | Pressure (kPa) | Company |
|---|---|---|---|---|---|---|
| **CMS** | MSC-3K 162 [1] | 0.58 | 5.88 | 303 | 100 | Takeda Chemical Industries Ltd. |
| | MSC-3K 172 [2 | 0.25 | 2.2 | 303 | 105 | |
| | MSC-3A from coconut shells [3] | 0.97 | 4.9 | 303 | 800 | |
| **Titanosilicate** | Sr-ETS-4 (activated at 588 K) [4] | 12.5 | 20 | 295 | 100 | BASF |
| | Sr-UPRM-5 (TEA) (activated at 493 K) [5] | 1.95 | 25.42 | 298 | - | Developing-phase in the USA |
| | Ba-ETS-4 (activated at 673 K) [6] | 3.36 | 205.3 | 283 | 700 | No further work was pursued |
| **AC/CMS** | PET-DC-0 [7] | 3.85 | 50 | 298 | 100 | |
| **MOF** | MIL-100 (Cr) [8] | 2.05 | 3.9 | 283 | 100 | Materials of Institut Lavoisier |
| **Zeolite** | Mg-Clinoptilolite [4] | 0.56 | 10 | 295 | 100 | Steelhead Speciality Minerals |
| **AC** | Norit- RB3 [9] | 0.30 | 0.34 | 273 | 100 | JMCD Australia Ltd. |

**References:**

1. Bae, Y.-S. and C.-H. Lee, Sorption kinetics of eight gases on a carbon molecular sieve at elevated pressure. Carbon, 2005. 43(1): p. 95-107.

2. Xiao, G., et al., Nitrogen rejection from methane using dual-reflux pressure swing adsorption with a kinetically-selective adsorbent. Chemical Engineering Journal, 2019. 372: p. 1038-1046.

3. Qinglin, H., S. Sundaram, and S. Farooq, Revisiting transport of gases in the micropores of carbon molecular sieves. Langmuir, 2003. 19(2): p. 393-405.

4. Jayaraman, A., et al., Clinoptilolites for nitrogen/methane separation. Chemical Engineering Science, 2004. 59(12): p. 2407-2417.

5. Yu, M., et al., Selective adsorption of N2 over CH4 in flexible Sr2+- and Ba2+-UPRM-5 (TEA) titanium silicates: Effect of activation temperature. Chemical Engineering Journal, 2014. 252: p. 311-319.

6. Majumdar, B., et al., Adsorption and diffusion of methane and nitrogen in barium exchanged ETS-4. Industrial & engineering chemistry research, 2011. 50(5): p. 3021-3034.

7. Cansado, I.P., et al. Activated carbons prepared from natural and synthetic raw materials with potential applications in gas separations. in Advanced Materials Research. 2010. Trans Tech Publ.

8. Yoon, J.W., et al., Selective nitrogen capture by porous hybrid materials containing accessible transition metal ion sites. Nature materials, 2017. 16(5): p. 526-531.

9. Lu, W., et al., Rejecting N2 from natural gas by dual reflux pressure swing adsorption with activated carbon. Journal of Natural Gas Science and Engineering, 2020. 81: p. 103457.

# Appendix H - Energy balance window

The energy balances which accurately represents the heat exchanges of a non-isothermal system with compressible flow are equation (1) for the fluid phase, equation (2) for the solid phase and equation (3) for the bed wall [1].

$$-k_g\varepsilon_i\frac{\partial^2 T_g}{\partial x^2}+C_{vg}v_g\rho_g\frac{\partial T_g}{\partial x}+P\frac{\partial v_g}{\partial x}+C_{vg}\rho_g\varepsilon_t\frac{\partial T_g}{\partial t}+H_s a_p\left(T_g-T_s\right)+H_w\frac{A_{Hi}}{V_{Hi}}\left(T_g-T_w\right)=0 \quad (1)$$

This equation is divided in six terms, in order of appearance: the axial thermal conduction, convection, P-V work compression, thermal accumulation in gas phase, heat transfer between the fluid and the adsorbent and heat transfer between the gas and the internal wall of the adsorber. Additionally, $T_g,\ T_s\ and\ T_w$, respectively, represent the gas, solid and wall temperatures, $k_g$ is the fluid thermal conductivity, $C_{vg}$ is the fluid heat capacity, $\rho_g$ stands for the gas density, $H_s$ and $H_w$ are the heat transfer coefficients of the fluid/solid and fluid/wall, respectively, the specific surface area of adsorbent is defined as $a_p$, while $A_{Hi}$ and $V_{Hi}$ are relative to the internal wall, whereas the first corresponds to the area and the second to the volume available for heat transfer.

Relatively to the solid phase energy balance, it involves four terms: axial thermal conduction, thermal accumulation in this phase, thermal accumulation due to the heat released during adsorption and heat transfer between gas and solid.

$$-k_s\frac{\partial^2 T_s}{\partial x^2}+C_{ps}\rho_b\frac{\partial T_s}{\partial t}+\rho_p\sum\nolimits_i\left(\Delta H_i\frac{\partial q_i}{\partial t}\right)-H_s a_p\left(T_g-T_s\right)=0 \quad (2)$$

Here, relatively to the adsorbent, $k_s$ is its thermal conductivity, $C_{ps}$ is its heat capacity and $\Delta H_i$ represents its adsorption enthalpy for component $i$.

Ultimately, considering the wall energy balance, four terms are applicable: axial thermal conduction along the wall, heat accumulation in the wall, gas/wall and wall/environment heat transfer.

$$-k_w\frac{\partial^2 T_w}{\partial x^2}+C_{pw}\rho_w\frac{\partial T_w}{\partial t}-H_w\frac{A_{Hi}}{V_{He}}\left(T_g-T_w\right)+H_{amb}\frac{A_{He}}{V_{He}}\left(T_w-T_{amb}\right)=0 \quad (3)$$

Here, relatively to the wall, $k_w$ is its thermal conductivity, $C_{pw}$ is its heat capacity, $\rho_w$ its density, $A_{He}$ and $V_{He}$ the external wall area and volume for heat transfer and $H_{amb}$ and $T_{amb}$ represent the heat transfer for wall/environment and the environmental temperature.

Reference

1. Aspen Technology, Aspen Adsim 2004.1, Adsorption Reference Guide. 2005.

# Appendix I - Breakthrough curve for pure $CH_4$ on Norit RB-3

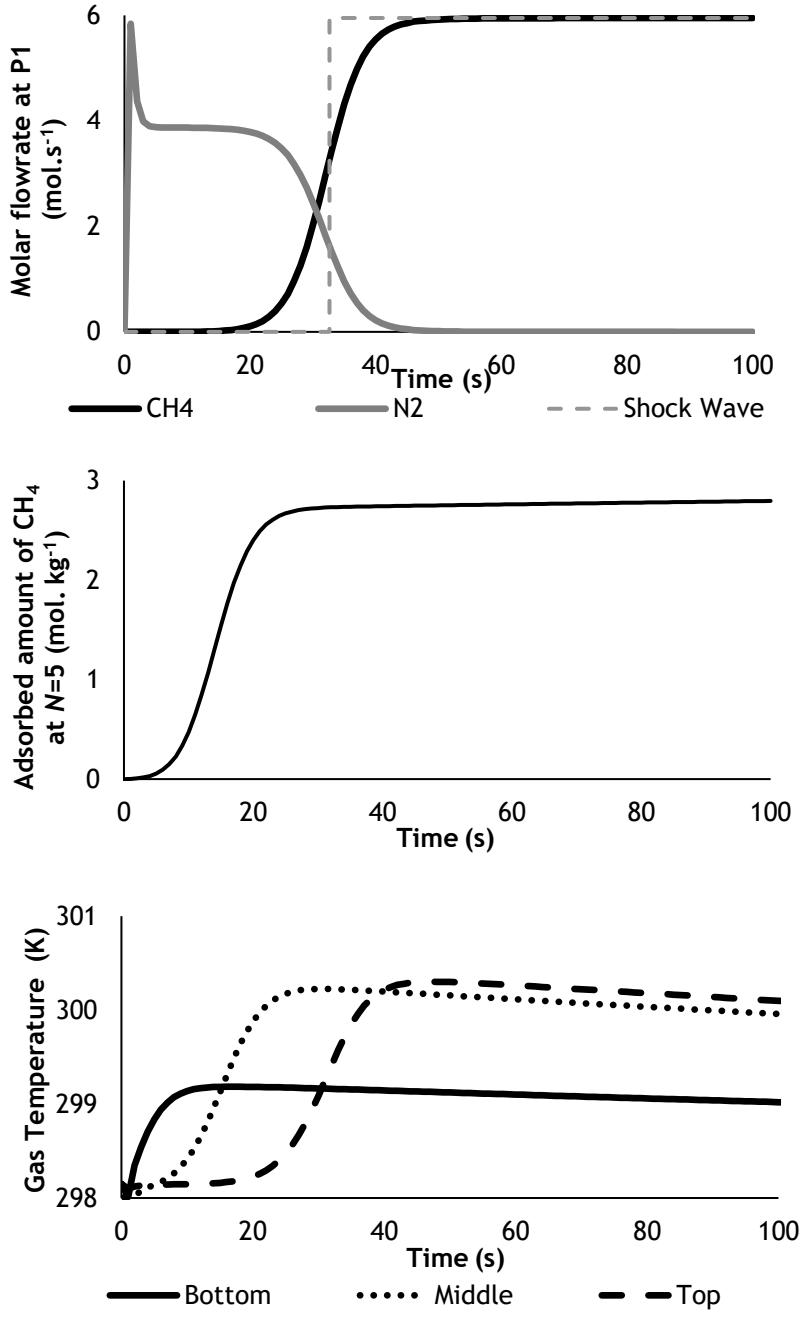


*Figure 1. Simulation results for the pure $CH_4$ breakthrough curve for F=500 $Nm^3.h^{-1}$, D=0.27 m, L=1.37 m, $U_s$=0.23 $m.s^{-1}$ where a) molar flowrate history at P1; b) solid loading in the adsorbent at the middle of the bed (N=5); c) gas phase temperature along the column.*

# Appendix J - Breakthrough curve additional analysis for CMS-3K 172

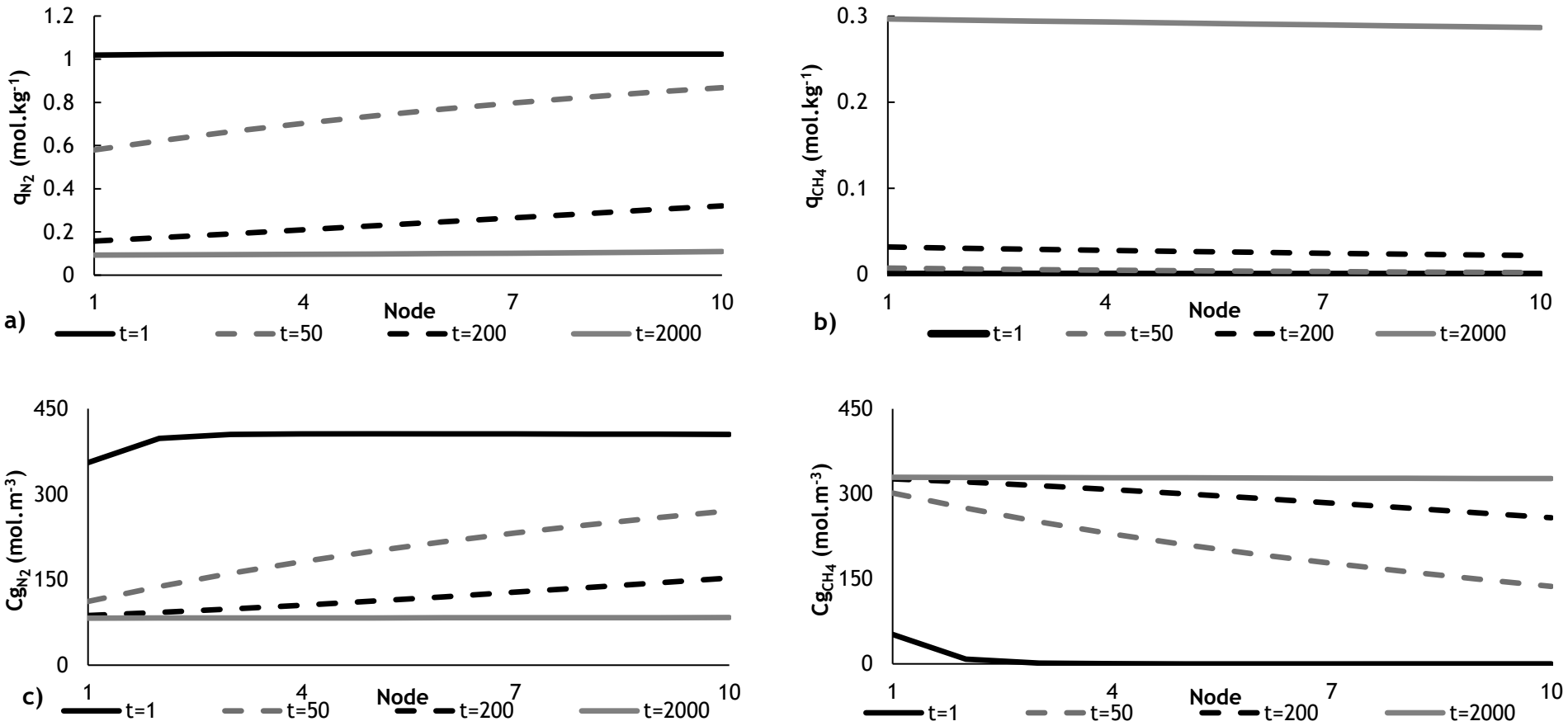


*Figure 1. Simulation results for the binary breakthrough curve for a flowrate of 500 $Nm^3.h^{-1}$, D=0.80 m, L=2.41 m, $v_s$=0.03 $m.s^{-1}$ where it is represented the evolution of the solid phase for $N_2$ (a) and for $CH_4$ (b) and the gas phase concentration profiles for $N_2$ (c) and for $CH_4$ (d).*

# Appendix K - Simulation results for the run (4) of the 8-step optimized configuration

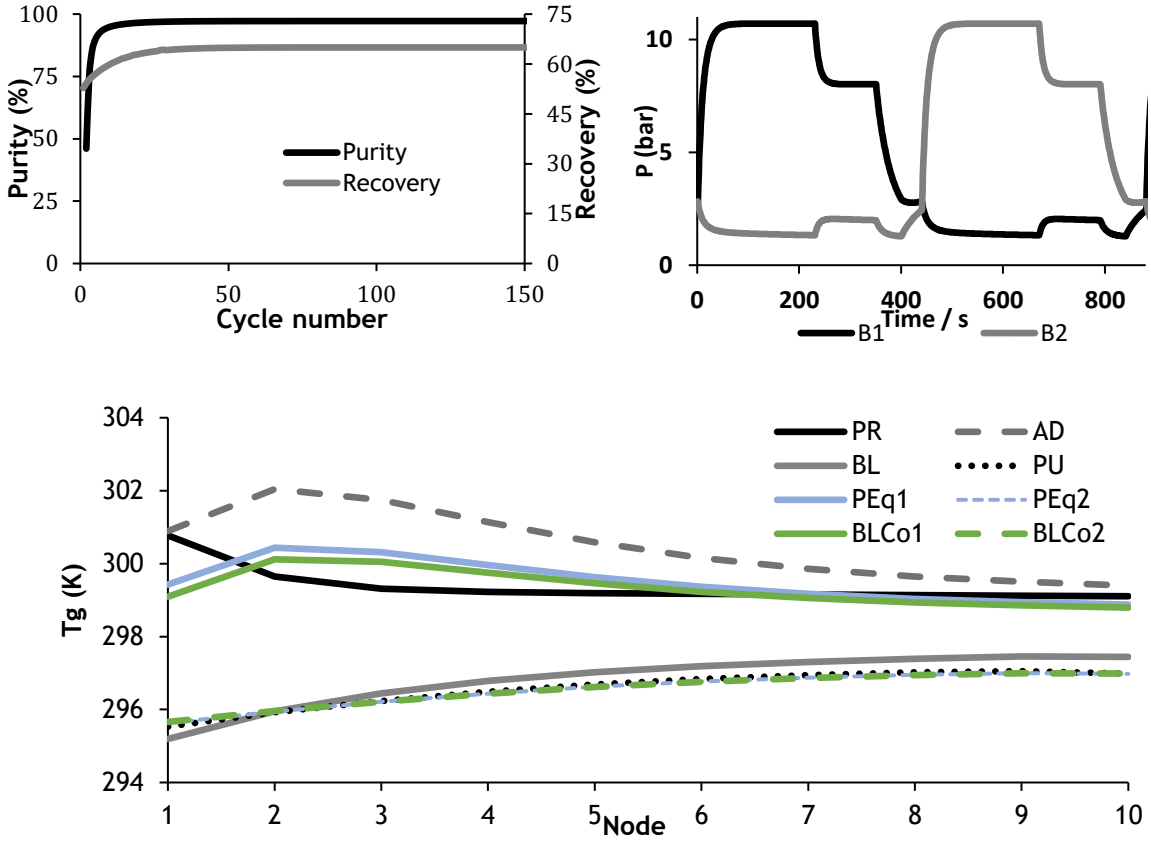


*Figure 1. Simulation results for the 8-step PSA optimized run (4) where: a) evolution of the $CH_4$ purity and recovery with the cycle number; b) pressure obtained at the column outlet at CSS; c) Gas temperature profile along the bed at the end of each step at CSS.*

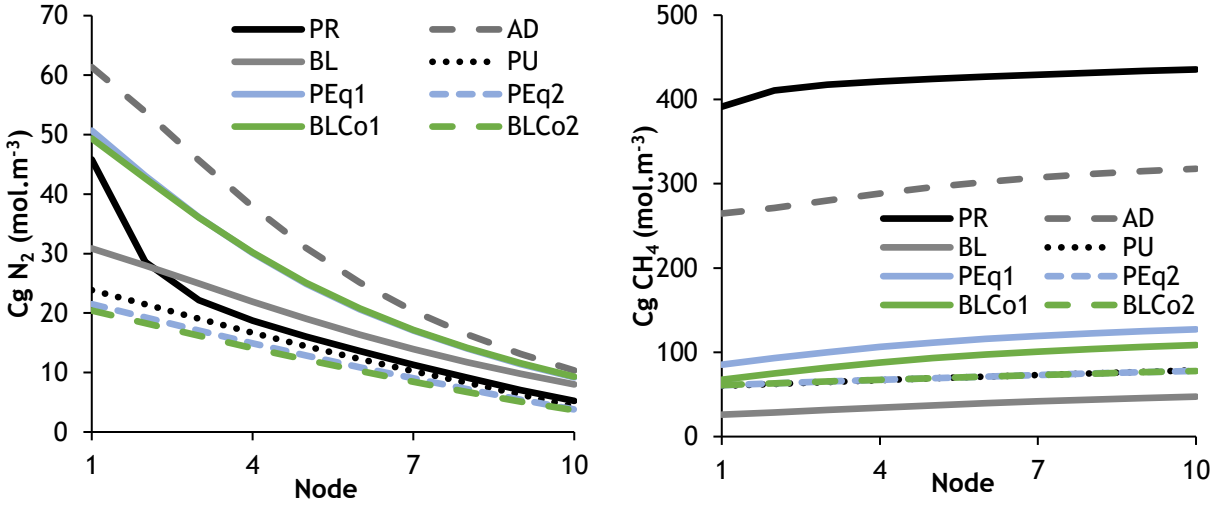

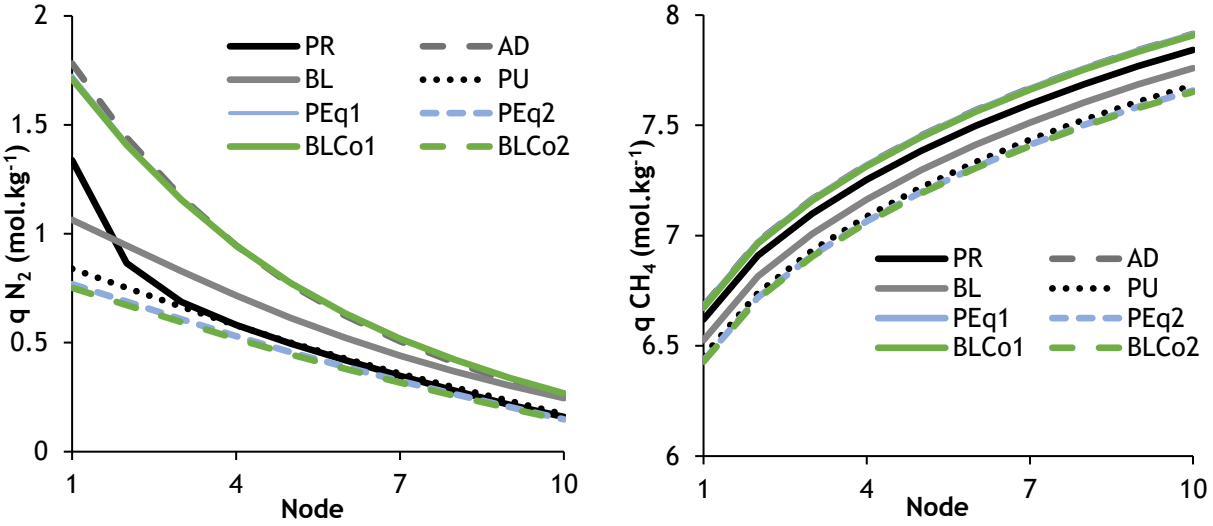


*Figure 2. Gas phase (a and b) and solid phase (c and d) concentration profiles for $N_2$ (a and c) and $CH_4$ (b and d) at CSS obtained for the 8-step PSA optimized run (4).*